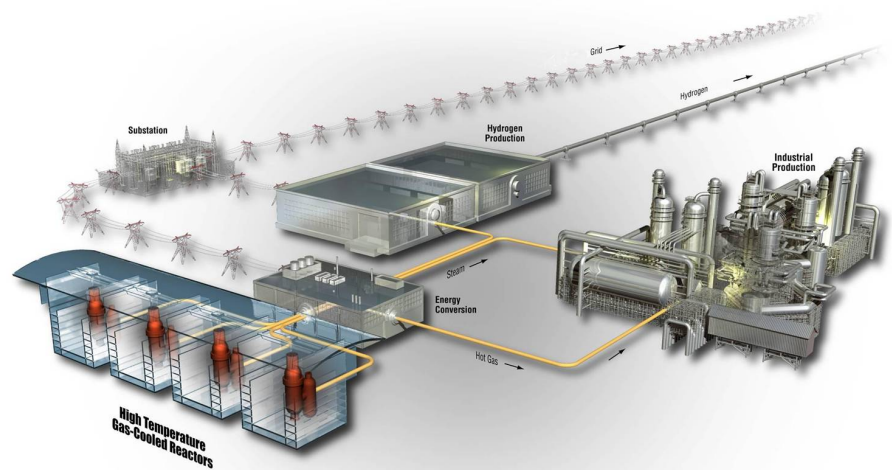


Reactor Physics Characterization of the HTR Module with UCO Fuel

Gerhard Strydom

January 2011

The INL is a
U.S. Department of Energy
National Laboratory
operated by
Battelle Energy Alliance



DISCLAIMER

This information was prepared as an account of work sponsored by an agency of the U.S. Government. Neither the U.S. Government nor any agency thereof, nor any of their employees, makes any warranty, expressed or implied, or assumes any legal liability or responsibility for the accuracy, completeness, or usefulness, of any information, apparatus, product, or process disclosed, or represents that its use would not infringe privately owned rights. References herein to any specific commercial product, process, or service by trade name, trade mark, manufacturer, or otherwise, does not necessarily constitute or imply its endorsement, recommendation, or favoring by the U.S. Government or any agency thereof. The views and opinions of authors expressed herein do not necessarily state or reflect those of the U.S. Government or any agency thereof.

Reactor Physics Characterization of the HTR Module with UCO Fuel

Gerhard Strydom

January 2011

**Idaho National Laboratory
Next Generation Nuclear Plant Project
Idaho Falls, Idaho 83415**

**Prepared for the
U.S. Department of Energy
Office of Nuclear Energy
Under DOE Idaho Operations Office
Contract DE-AC07-05ID14517**

Next Generation Nuclear Plant Project

Reactor Physics Characterization of the HTR Module
with UCO Fuel

INL/EXT-10-20521

January 2011

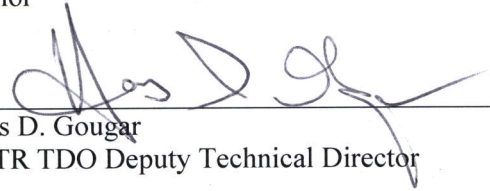
Approved by:



Gerhard Strydom
Author

01/12/2011

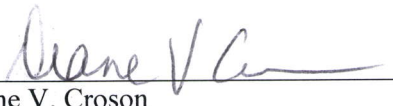
Date



Hans D. Gougar
VHTR TDO Deputy Technical Director

01/13/2011

Date



Diane V. Croson
VHTR TDO Deputy Director

1/13/11

Date

SUMMARY

The high temperature reactor (HTR) module¹ is a graphite-moderated, helium cooled pebble bed design that has been extensively used as a reference template for the former South African and current Chinese HTR² programs. This design utilizes spherical fuel elements packed into a dynamic pebble bed, consisting of tri-structural isotropic coated uranium oxide (UO₂) 500 μm fuel kernels with a U-235 enrichment of 7.8% and a heavy metal loading of 7 grams per pebble. The main objective of this study was to compare several important reactor physics and core design parameters for the HTR module and an identical reactor design utilizing 425 μm UCO fuel kernels with a U-235 enrichment of 14%. Fuel kernels of this type are currently being tested in the Idaho National Laboratory's Advanced Test Reactor as part of the larger Next Generation Nuclear Plant project. The PEBBED-THERMIX³ code, which was developed specifically for the analysis of pebble bed HTRs, was used to compare the coupled neutronic and thermal fluid performance of the two fuel particle designs. The following parameters were compared for seven defined cases:

- *Steady-state*: k-eff, control rod worths, power and flux profiles, fuel and moderator temperatures, and power peaking factors.
- *Design basis accidents*: maximum fuel temperatures during a depressurized loss of forced cooling (DLOFC) event, as well as the reactivity behavior for a water/steam ingress scenario.

The first three cases compared the HTR-Module fuel (Case 1) with fuel of the same UO₂ TRISO particle design with enrichment increased to 14% (Case 2) and UCO TRISO fuel as described above. For these three cases the sphere heavy metal loading and average number of passes through the core remained constant at 7 grams and 15 passes. The analysis of the normal operation (steady state) equilibrium results for these three cases showed that the dominant contributor to the observed variances between the HTR module UO₂ and UCO cores is the increase in the U-235 enrichment to 14%, and not the additional moderation effects of the oxygen to carbon exchange. The flux, power density, and temperature data of Case 2 are very similar to the results of Case 3 - certainly within the expected uncertainty margins of these calculations. Although the UCO core displayed higher power densities, it was not carried through to the fuel temperatures where the differences were minimal.

The use of UCO fuel at 14% enriched and 176 MWd/kg U/18.8% FIMA average discharge burnup (Case 3) lead to a small increase of 48°C (3%) in the DLOFC peak fuel temperature to 1533°C. If typical uncertainty margins between 61°C (4%) and 107°C (7%) are taken into account, the fuel temperatures are still below 1650°C. However, it was also shown that only 4% of the 360,000 fuel spheres in the core have maximum temperatures above 1400°C. It was also confirmed that the DLOFC fuel temperature data for Cases 2 and 3 are essentially identical, indicating that the change from UO₂ to UCO fuel kernels is not the determining factor for the DLOFC fuel temperatures, but rather the change in enrichment and the resultant higher burnup achieved.

For the steam ingress scenario, it was found that the UCO-fueled core is almost twice as reactive as the UO₂-fueled core (Case 3 peak value 3.21% at 3,300 kg steam vs. Case 1 peak value 1.63% at 1,980 kg steam). However, the control rod shutdown worths for a full SCRAM were also compared for these two cases (5.6% for Case 1 and 4.8% for Case 3), and it was concluded that an acceptable shutdown margin exist for both of these cases. However, given the much larger positive reactivity insertion, a transient analysis would also be required to compare peak power and temperature.

The reactivity insertion values for 600 kg of steam was also compared with the reactivity added from a full control rod withdrawal, as was done for the HTR module SAR. A full withdrawal lead to reactivity increases of 1.21% (Case 1) and 1.49% (Case 3), vs. steam ingress values of 0.99% and 1.42%.

The control rod withdrawal event for both these cases (UO₂ and UCO fueled cores) is therefore the bounding case for reactivity insertion design basis accidents, supporting the original HTR module design intentions.

The analysis of these two accidents, together with the acceptable results obtained from the steady-state and control rod worth analysis, lead to the conclusion that the 425µm 14% enriched UCO TRISO particle is a feasible design option that stays within the reactor physics critical safety envelopes. It should however be noted that the fuel performance of this core design was beyond the scope of this study, and care should be taken not to equate acceptable neutronics and thermal fluid behavior with acceptable levels of fission product release rates, since many more phenomena are involved in this aspect of fuel design. These phenomena are being addressed within the scope of the NGNP/AGR Fuel Development and Qualification Program.

CONTENTS

SUMMARY	iv
1. INTRODUCTION	1
2. OVERVIEW OF HTR MODULE DESIGN AND COMPUTATIONAL TOOLS	2
2.1 HTR Module Layout	2
2.2 Computational Tools and Models	4
3. RESULTS	6
3.1 Case Descriptions	6
3.2 Steady-State Results	7
3.2.1 Flux Comparisons	9
3.2.2 Power Density Comparisons	14
3.2.3 Temperature Comparisons	19
3.2.4 Control Rod Worth Comparisons	23
3.3 DLOFC Results	23
3.4 Water Ingress Results	27
4. SUMMARY AND CONCLUSIONS	31
5. REFERENCES	33

FIGURES

Figure 1. Cross-section layout of the HTR module. ⁴	2
Figure 2. TRISO fuel particle.	4
Figure 3. Comparison between the Case 1 axial power density (MW/m ³) and fuel temperature profiles at r = 15 cm.	8
Figure 4. Case 1 fast flux (n/cm ² .s)	10
Figure 5. Case 3 fast flux (n/cm ² .s)	10
Figure 6. Case 1 thermal flux (n/cm ² .s).	11
Figure 7. Case 2 thermal flux (n/cm ² .s).	11
Figure 8. Case 3 thermal flux (n/cm ² .s).	12
Figure 9. Case 4 thermal flux (n/cm ² .s).	12
Figure 10. Case 5 thermal flux (n/cm ² .s).	13
Figure 11. Case 6 thermal flux (n/cm ² .s).	13
Figure 12. Case 7 thermal flux (n/cm ² .s).	14
Figure 13. Case 1 power density (W/cm ³).	15
Figure 14. Case 2 power density (W/cm ³).	15
Figure 15. Case 3 power density (W/cm ³).	16

Figure 16. Case 4 power density (W/cm^3).	16
Figure 17. Case 5 power density (W/cm^3).	17
Figure 18. Case 6 power density (W/cm^3).	17
Figure 19. Case 7 power density (W/cm^3).	18
Figure 20. Cases 1–7 radial power density (MW/m^3) at $z = 344$ cm.	18
Figure 21. Cases 1–7 axial power density (MW/m^3) at $r = 15$ cm.	19
Figure 22. Case 1 solid material temperature ($^{\circ}C$) – 2D contour plot.	20
Figure 23. Case 3 solid material temperature ($^{\circ}C$) – 2-D contour plot.	20
Figure 24. Cases 1–6 axial solid material temperature ($^{\circ}C$) at $r = 7.5$ cm.	21
Figure 25. Cases 1–6 radial solid material temperature ($^{\circ}C$) at $z = 450$ cm.	21
Figure 26. Fuel sphere shell temperatures ($^{\circ}C$) at core location ($r;z$) = (7.5 cm;451 cm).	22
Figure 27. Cases 1–6 DLOFC maximum fuel temperature ($^{\circ}C$) vs. time.	24
Figure 28. Cases 1–6 DLOFC maximum fuel temperature ($^{\circ}C$) vs. time – detail of the time spent above $1400^{\circ}C$.	25
Figure 29. Cases 1–7 maximum fuel temperature volumetric distribution (% of total fuel volume).	26
Figure 30. Cases 1–6 reactivity addition (%) because of water ingress (kg).	28
Figure 31. Cases 1–3 reactivity addition (%) because of water ingress (kg).	30

TABLES

Table 1. HTR module design data.	3
Table 2. UO_2 and UCO fuel kernel data.	3
Table 3. HTR module PEBBED case summary.	6
Table 4. Cases 1–7 steady-state results.	7
Table 5. Fuel sphere shell temperatures ($^{\circ}C$) at core location ($r;z$) = (7.5 cm;451 cm).	22
Table 6. Cases 1–7 Control Rod Worths.	23
Table 7. Cases 1–7 DLOFC results.	24
Table 8. Cases 1–7 maximum fuel temperature volumetric distribution (% of total fuel volume).	25
Table 9. Cases 1–7 water ingress results.	28

Reactor Physics Characterization of the HTR Module with UCO Fuel

1. INTRODUCTION

The HTR module¹ is a graphite-moderated, helium cooled pebble bed high temperature reactor (HTR) design that has been extensively used as a reference point for the former South African² and current Chinese HTR³ programs. This design utilized spherical fuel elements packed into a dynamic pebble bed consisting of tri-structural isotropic (TRISO) coated uranium oxide (UO₂) fuel kernels with a U-235 enrichment of 7.8% and a heavy metal loading of 7 grams per pebble.

The main objective of this study is to compare several important reactor physics and core design parameters for the HTR module and an identical design utilizing UCO (uranium oxycarbide) fuel kernels. Fuel kernels of this type are currently being tested in the Idaho National Laboratory's (INL) Advanced Test Reactor as part of the larger Next Generation Nuclear Plant (NGNP) project. The primary advantage of using this fuel is in the increased fuel utilization that can be reached (higher burnup before discharge) because of the lower carbon monoxide plus gaseous fission product load at high burnup levels.

Seven cases, varying the total heavy metal loading and number of fuel passes, were analyzed, and recommendations are made for achieving a feasible UCO-fueled HTR module design from a reactor physics point of view. This study is not intended to provide a comprehensive core design characterization because it does not provide accident scenarios, Xenon stability, reactivity coefficients, start-up analysis, fuel performance, etc.

2. OVERVIEW OF HTR MODULE DESIGN AND COMPUTATIONAL TOOLS

2.1 HTR Module Layout

A cross-section layout of the HTR module is presented in Figure 1. The primary design data for the HTR module and its fuel are summarized in Table 1.

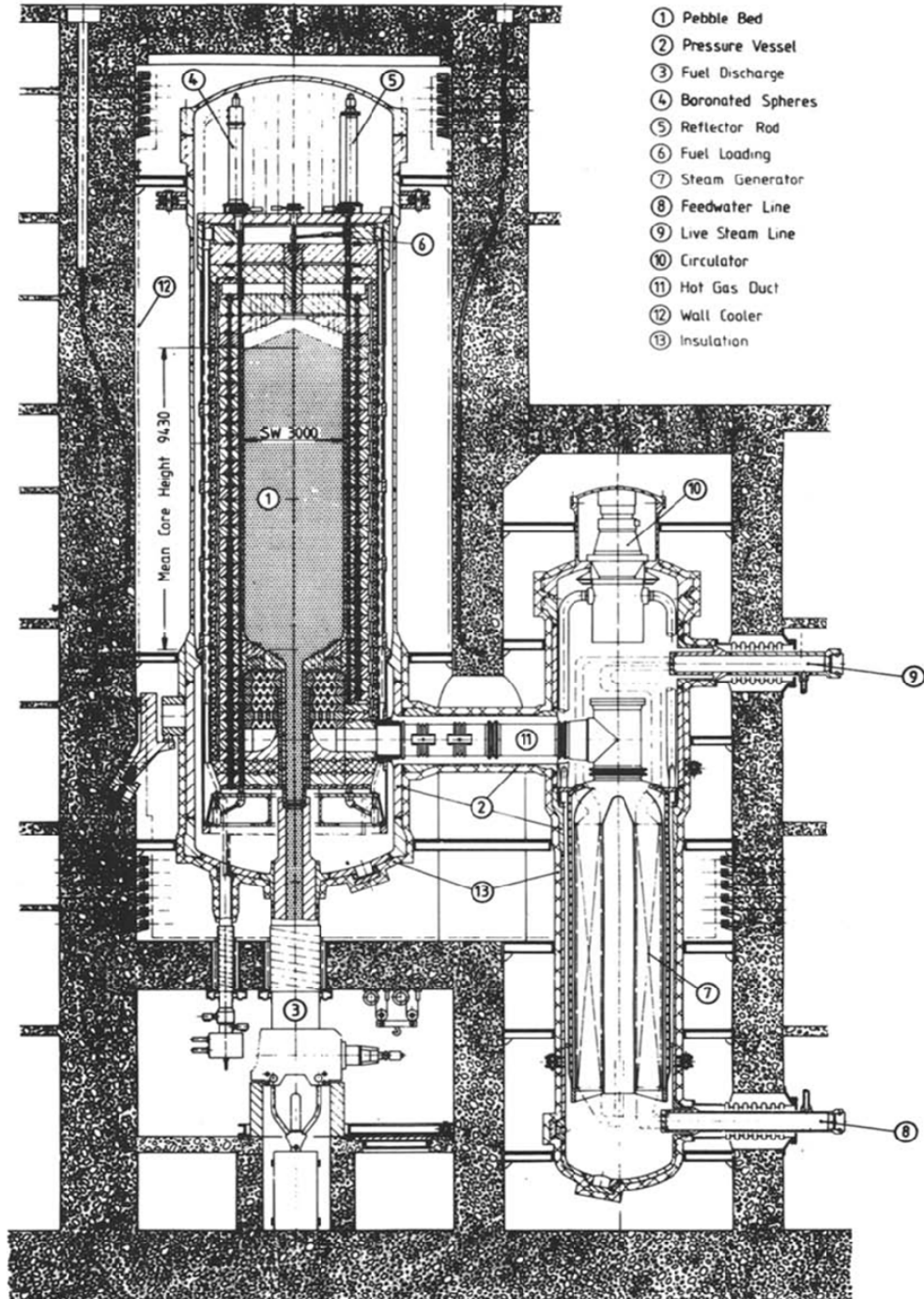


Figure 1. Cross-section layout of the HTR module.⁴

Table 1. HTR module design data.⁴

Parameter	Unit	Value
System Data		
Thermal power	MW	200
Core diameter	m	3.0
Core height	m	9.43
Inlet/outlet helium gas temperature	°C	250/750
Inlet/outlet steam temperature	°C	170/530
System pressure	MPa	6.0
Helium flow rate	kg/s	85
Fuel Data		
Number of fuel spheres		360,000
Number of TRISO particles per fuel sphere		11,600
U-235 enrichment	%	7.8
Heavy metal loading per fuel sphere	g	7
Average number of fuel passes through core		15
Average discharge burnup	MWd/kg U	80

The data for the UO₂ and UCO fuel kernels used in this study are summarized in Table 2, while an electron microscope photograph of a typical TRISO fuel kernel is shown in Figure 2. Note that the UO₂ and UCO fuel kernels are both coated with identical layers, i.e., the only differences are the smaller UCO kernel diameter and the higher UCO U-235 enrichment.

Table 2. UO₂ and UCO fuel kernel data.⁵

Parameter	Unit	Value for Fuel Kernel Type	
		UO ₂	UCO
Mean kernel diameter	µm	500	425
Mean buffer thickness	µm	100	100
Mean inner PyC thickness	µm	40	40
Mean SiC thickness	µm	35	35
Mean outer PyC thickness	µm	40	40
U-235 enrichment	%	7.8	14
Number of kernels in a fuel sphere (for a heavy metal loading of 7 g per sphere)		11,600	19,000

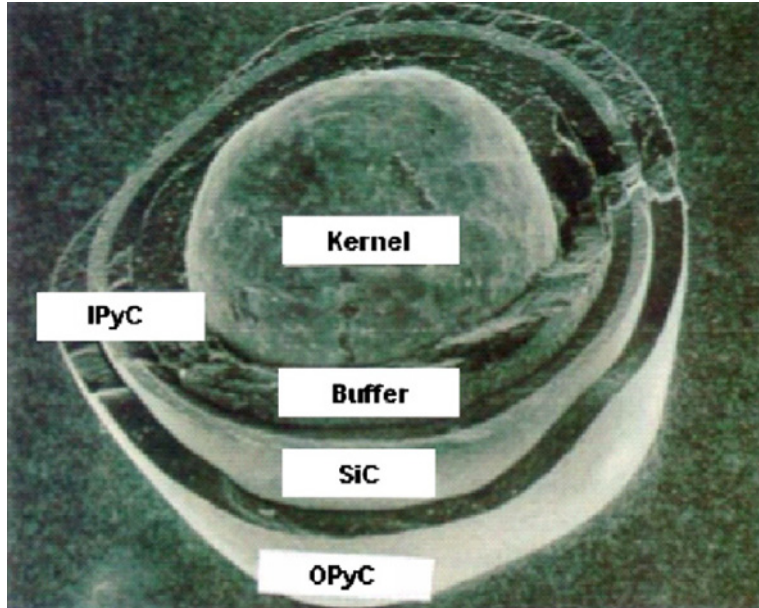


Figure 2. TRISO fuel particle.⁶

2.2 Computational Tools and Models

This study utilized a combination of three reactor physics codes: PEBBED⁷ for pebble-bed reactor design and fuel cycle analysis, THERMIX-KONVEK⁸ for thermal fluid analysis, and COMBINE-6⁹ for cross section preparation. PEBBED is used for self-consistent analysis of neutron flux and isotopic depletion and buildup in a pebbled bed HTR. The code can treat arbitrary pebble circulation schemes, and it permits more than one type of pebble to be specified. PEBBED was applied to the two-zone PBMR-268 concept and a very high temperature reactor core suitable for driving a hydrogen production plant.^{10,11} Output from PEBBED includes the spatial distribution of the burnup and of the principal nuclides throughout the reactor core and in the discharged pebbles.

The THERMIX-KONVEK code was specifically developed in Germany during the German HTR program for the thermal fluid analysis of pebble bed HTRs. It is capable of solving conduction and convection heat transfer in 2-D, and includes a simplified treatment of the radiative heat transport between the core structures. The code can also predict the time-dependent conduction heat transport during a depressurized loss of forced cooling (DLOFC) by assuming that all convection terminates instantaneously.

The COMBINE code solves the B-1 or B-3 approximation to the Boltzmann transport equation in 1-D for a homogeneous bare slab. COMBINE has recently been modified to support multiscale pebble bed reactor core simulation. The B-3 transport equation is now solved over the entire spectrum with simultaneous upscattering and resonance treatments in 167 energy groups. User-supplied buckling terms can reflect net inward or outward leakage. COMBINE accepts separate kernel-to-kernel (intrapebble) and pebble-to-pebble (interpebble) Dancoff factors generated by the PEBDAN code to account for shadowing. A 1-D discrete ordinates transport (ANISN) solver has been embedded in the code to capture spatial effects. With pebble bed geometry in mind, COMBINE employs a multistage homogenization process that minimizes the error inherent in the multigroup approximation. Explicit transport models of the TRISO particle, pebble, and radial core wedges are solved in 167 groups before being coalesced in energy and space to generate few group cross sections for PEBBED.

Axial and azimuthal leakages are still treated with transverse buckling terms. Radial leakage, the dominant contributor to leakage from the spectral zones, is captured explicitly in the core transport stage and in 167 groups. The source for the radial reflector regions, including control rods, is the true current emanating radially from the core region with adjustments for axial and azimuthal effects.

The implementation of the multistage approach to homogenization in COMBINE enables the explicit modeling of the different structures that are present. For the pebble bed itself, the transport equation is solved in spherical geometry, first for the TRISO particles and then for the pebbles and surrounding coolant. For the bulk of the reflector and core barrel, explicit geometrical models are not required because these regions are largely homogeneous. For control rod zones, a transport model is solved in cylindrical coordinates. Control rods in most pebble bed reactor designs consist of an annulus of boron carbide sandwiched between alloy tubes. These tubes are lowered into holes drilled vertically into the side reflector near the core. The geometry of the rods is captured explicitly except for the surrounding graphite reflector. The reflector is modeled as an annulus with a thickness that is specified by the user.

The PEBBED-THERMIX models used in this study are all based on the HTR module design¹ and Cases 1–7 share identical geometry, material definitions, and THERMIX files. The only variations per case are:

- The updated fuel number densities, number of passes, and heavy metal loading for Cases 2–7.
- Updated cross sections for each case, generated by COMBINE.

All model inputs are best estimates, i.e., no conservatism or uncertainty margins were added. A possible exception to this is the modification to allow 10% reactor bypass flow through the control rod channel. This factor can be seen as a conservatism (since, by design, all flow should flow through the core for optimal energy transfer, and not just 90%), or as a realistic representation of an operating reactor (e.g., control rod cooling is generally required for HTR designs, and leaks between the reflector graphite blocks cannot be completely closed). Most previous HTR studies accept a bypass flow of 10% as a realistic/best estimate assumption, compared to values up to 20% for conservative bypass flow cases.

The remaining model approximations and simplifications include:

- The deposition of heat in the reflector structures (gamma and fast neutrons) is not included. This amounts to approximately 6% of the total power generation in a typical HTR design,¹² and influences the fuel and reflector temperatures during a DLOFC, reactivity coefficients, and control rod worths.
- The thermal conductivity of graphite is a temperature and fluence dependent function that decreases with fast neutron damage exposure. All of the data in this study is generated using zero fluence exposure, which implies high thermal conductivities. This approach is considered appropriate for comparing the relative performance of the cases studied, but will not typically result in best estimate DLOFC fuel temperatures later in the plant life.
- The thermal physical properties of the UCO fuel kernels are not included in this study, i.e., the specific heat and thermal conductivities used are all UO₂ values. The effect is judged to be only important for very fast reactivity insertion events, since the fuel kernels are usually in close equilibrium with the surrounding graphite matrix during normal operation and slow transients. The change in nuclide number densities (the exchange of oxygen for carbon) is, however, explicitly taken into account during the COMBINE and PEBBED neutronics.

The power peaking effects of random fresh fuel clustering within the pebble bed is not addressed in this scoping study, but it is expected that the use of higher enriched fuel will lead to larger variations in the reactivity and power densities between the fresh and a more burnt fuel.

3. RESULTS

3.1 Case Descriptions

The primary input data for the seven cases included in this study are presented in Table 3. All cases use the same HTR module operational envelope (Table 1), geometry (Figure 1), and material definitions. Cases 1 and 3 are the “baseline” HTR module cases, fueled with UO₂ and UCO respectively. The seven cases were designed to answer the following questions:

- *Case 1 and 3:* Can the HTR module be operated with higher enriched UCO fuel to a higher discharge burnup, instead of lower burnt UO₂ fuel, and will it still be within an acceptable safety envelope (e.g., reactivity, fuel temperatures, rod worths, etc.)?
- *Case 2:* What is the effect of simply using 14% enrichment on the HTR module with UO₂ fuel? How does this design compare with the 14% enriched HTR module with UCO fuel?
- *Cases 4 and 5:* What is the effect of the heavy metal loading on the operational parameters; specifically, on the water ingress scenario? Is 7 grams heavy metal per sphere, still an acceptable choice for the UCO-fueled HTR module, or should a lower loading be considered?
- *Cases 6 and 7:* To what degree can the (DLOFC) fuel temperatures be influenced by varying the number of cycles (fuel passes) through the core?

Table 3. HTR module PEBBED case summary.

Case #	1	2	3	4	5	6	7
Fuel kernel type	UO ₂	UO ₂	UCO	UCO	UCO	UCO	UCO
Heavy metal loading per fuel sphere (g)	7	7	7	9	5	7	7
U-235 enrichment (%)	7.8	14	14	14	14	14	14
Average discharge burn-up (MWd/kg U)	80	160	160	160	160	160	160
Kernel size (μm)	500	500	425	425	425	425	425
Average number of fuel passes through core	15	15	15	15	15	20	10
Number of TRISO particles per fuel sphere	11,600	11,600	19,000	24,450	13,550	19,000	19,000
Fuel flow rate (spheres per day)	5,350	2,857	2,600	2,050	5,400	3,810	1,700

For Case 3, the smaller kernel size of the UCO fuel, coupled with the slightly lower kernel mass caused by the increase in U-235 enrichment, results in more kernels required per sphere to achieve the same heavy metal loading (7 grams) as for Case 1. Each fuel sphere in Case 3 contains 19,000 fuel kernels, which averages 7,400 kernels per sphere more than Case 1. The higher UCO enrichment (14%) enables a higher burnup to be achieved before the fuel needs to be discharged; a target of 160 MWd/kg U (~17% fissions per initial metal atom) has been set for this study. Using the simple relationship 11¹¹

$$M = \frac{B_d m_{HM} f}{P} \quad (1)$$

with m_{HM} the heavy metal loading, f the daily pebble loading rate, and P the total thermal power, the average number of passes M that the fuel needs to pass through the core to reach the target discharge burnup B_d can be calculated. For comparison with HTR module UO₂ Case 1, the number of passes for Cases 2–5 has been kept at 15 passes, while the effect of the number of passes are analyzed in Cases 6 and 7.

The 7 grams heavy metal loading for the UO₂ HTR module fuel was determined by the trade-off between under and over-moderation (neutron economy) and the reactivity behavior of the core during a postulated water ingress scenario,¹ but an optimal moderation ratio needs to be determined for a change in the fuel such as this UCO-fueled core. Cases 4 and 5 are included here as a simplistic exploration of this aspect of core design, and in Section 3.4 the effect of steam entering the core is assessed for the 5, 7, and 9 gram heavy metal loading scenarios.

3.2 Steady-State Results

The summarized steady-state (normal operation equilibrium core) results for Cases 1–7 are presented in Table 4 and the explanation following the table.

Table 4. Cases 1–7 steady-state results.

Case	1	2	3	4	5	6	7
k-eff	1.00006	0.99735	1.00003	0.99963	1.00014	1.00029	0.99980
Average discharge burn-up (MWd/kg U)	89	168	176	166	158	166	168
% fissions per initial metal atom	9.5	17.9	18.8	17.7	16.9	17.7	17.9
Discharged heavy metal content (g)	6.3	5.8	5.9	7.5	4.2	5.9	5.9
Average total core sphere flow recirculation rate (spheres per day)	4,993	2,649	2,412	2,089	5,201	3,509	1,722
Average fresh fuel loading rate (spheres per day)	357	199	161	139	260	175	172
Average core residence time (days)	1,010	1,807	2,242	2,585	1,039	2,052	2,092
Maximum pebble power (kW)	1.9	2.6	2.7	2.2	3.4	2.4	2.5
Peak core power density (MW/m ³)	5.6	6.0	6.5	6.7	6.2	5.9	6.4
Peak thermal flux (n/cm ² .s)	1.6E+14	1.5E+14	1.5E+14	1.4E+14	2.2E+14	1.5E+14	1.6E+14
Peak fast flux (n/cm ² .s)	1.6E+14	1.6E+14	1.7E+14	1.5E+14	1.7E+14	1.5E+14	1.7E+14
Maximum steady-state temperature (°C)	861	864	859	828	908	853	854
Maximum temperature difference over fuel sphere ($T_{\text{surface}} - T_{\text{center}}$) (°C)	63	92	97	82	118	83	92

The peak power generated per sphere is higher for UCO-fueled Case 3 (2.7 kW) when compared with the reference UO₂ Case 1 value of 1.9 kW. This is a spatially dependent parameter that usually occurs in the spatial mesh where the peak power density is calculated for the freshly loaded fuel, as shown in Figure 13 and Figure 14. Since the heavy metal content and number of passes is identical for Cases 1 and 3, the differences are caused by the higher U-235 enrichment and the larger variation in fissile material content and associated sphere power between a fresh sphere and a last pass sphere for Case 3.

This conclusion is supported by the almost identical results of Cases 2 and 3. There is a smaller difference in the peak core power densities (5.6 MW/m³ vs. 6.5 MW/m³), and slight spatial variances in the radial power distributions of the Case 1 UO₂ and Case 3 UCO-fueled cores as shown in Figure 13 and Figure 15. These differences are discussed in more detail in Section 3.2.2.

The difference in power densities between Cases 1 and 3 are not observed in the maximum steady-state temperatures, e.g., Case 1 (861°C) is only 2°C higher than Case 2 (859°C). This is caused by the difference in the power/flux profiles and the fuel temperature profiles, i.e., the two data points (peak power and peak temperature) do not occur at the same spatial location. This aspect is shown in Figure 3, where the axial power and temperature shapes are compared for Case 1. It can be seen there that the power peak are located almost 6 meters higher in the core than the peak fuel temperature. This

downwards shift in the temperatures is caused by the forced heat removal via the helium gas, which enters the core from the top.

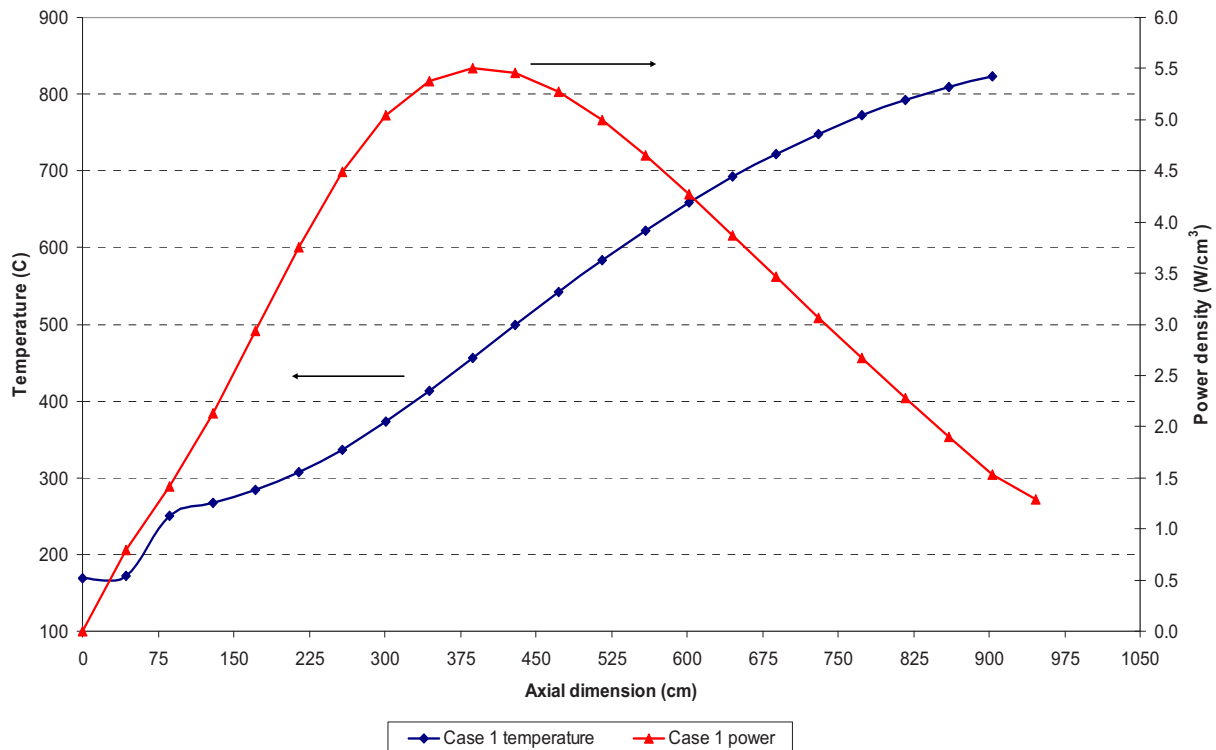


Figure 3. Comparison between the Case 1 axial power density (MW/m³) and fuel temperature profiles at r = 15 cm.

The higher and lower heavy metal loading (Cases 4 and 5) produced lower and higher peak power densities, respectively, since more (or less) fuel kernels had to produce the same overall total power in both cases. The fuel therefore “worked” harder for the 5 g heavy metal case, compared to the 9 g heavy metal case. This can also be seen in the maximum fuel temperatures for the two cases, where a difference of 80°C exists; and in the peak temperature gradient over the fuel spheres, where 36°C delta is calculated. It should however be noted that the radial power shapes (Figure 16 and Figure 17) for Cases 4 and 5 differ significantly, and specifically that the peak power for Case 4 is generated in the center of the core, while the peak power for Case 5 is generated at the outer edge of the core, next to the side reflector. (These differences are discussed in more detail in Section 0 and 3.2.2).

The effect of more (Case 6) or less (Case 7) passes through the core can be seen in the lower/higher power densities, since a higher number of passes leads to a less peaked axial power profile (compare the profiles for Cases 6 and 7 in Figure 21). Because of the convective effects, only a small decrease exists in the steady-state maximum fuel temperatures, but a large gain is obtained for the DLOFC fuel temperatures (see Figure 27). The power smoothing “gain” between 10 and 15 passes is not as significant as the gain between 15 and 20 passes (Cases 3 and 6).

3.2.1 Flux Comparisons

The fast flux shape (presented in Figure 4 for Case 1) does not vary significantly between the seven cases, and is typical of the cylindrical HTR designs. It reaches a peak value around $z = 400$ cm and tapers off fast in the reflector region as the neutrons are thermalized. Of interest here is the significant variance between Cases 1 and 7 in their thermal flux shapes, as shown in Figure 6 to Figure 12. The variations are at face value similar to the power density trends discussed in Section 3.2.2, but more pronounced, and not always in the same direction (e.g., compare the Case 3 thermal flux [Figure 8] and power density [Figure 15] shapes), since the reaction rate is the combined effect of the fast and thermal fluxes. All seven cases show a saddle shaped radial flux profile, with peaks at the inner core and side reflector regions. (The y-axis for all cases, except Case 5, was kept identical to enable easier visual comparisons). The following observations can be made:

- The reference HTR module case (Case 1) has symmetrical flux peaks at the core inner region and around 15 to 20 cm into the side reflector, whereas the UCO-fueled core (Case 3) exhibits a much larger peak in the reflector region. This thermal flux peak is the reason for the increased control rod worth in the UCO case. Table 6 shows that the withdrawal of all the control rods from their nominal location results in a reactivity increase of 1.49% for Case 3, whereas the rod withdrawal for Case 1 only leads to an increase of 1.21%.
- The effect of an increased heavy metal loading (Figure 9) can be clearly seen, with a depressed core thermal flux profile and a large peak in the reflector region. However, since this peak is still lower in amplitude than the reflector flux peak in Case 3, the reactivity insertion because of a total control rod withdrawal is less than Case 3 (see Table 6). The decrease in heavy metal loading to 5 g (see Figure 10) for Case 5 shows the expected inverse shape: a larger core region peak, and a lower reflector peak. In this case, since the fuel is working harder to produce 200 MW from 5 g of heavy metal, the thermal flux amplitudes are the highest of all seven cases, and this case also leads to the second largest reactivity insertion for a total control rod withdrawal (1.46%). The main cause of these changes is the change in moderation ratio that occurs when the heavy metal loading is varied.
- An increase in the number of fuel passes through the core (see Figure 11) flattens the axial thermal flux shape, but a larger thermal flux peak is produced in the reflector region because of increased thermalization. For the 10 pass Case 7 (see Figure 12), the thermal flux amplitude in the core is higher and more peaked towards the inner core region because of less parasitic absorption by fission product poisons and a larger fraction (1/10) of fresh fuel in a given core volume.

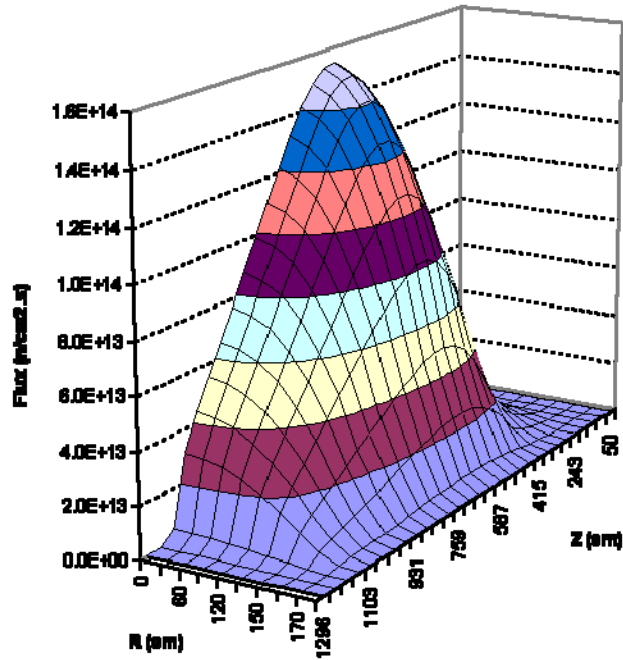


Figure 4. Case 1 fast flux (n/cm².s).

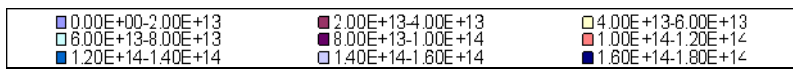
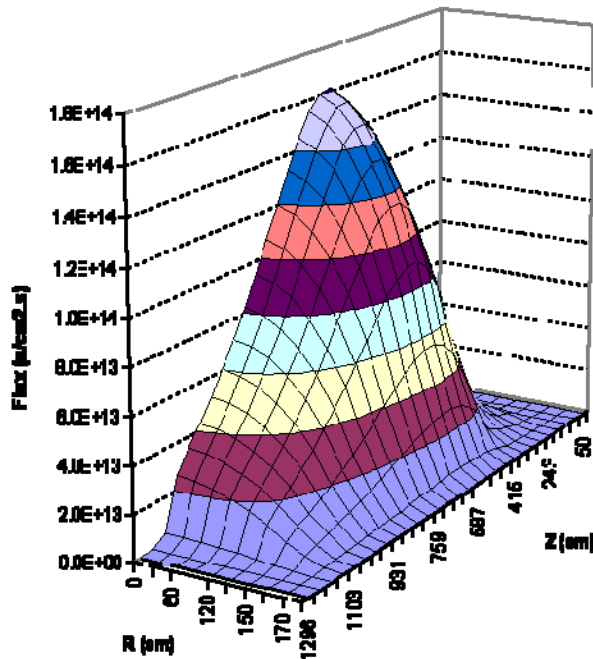


Figure 5. Case 3 fast flux (n/cm².s).

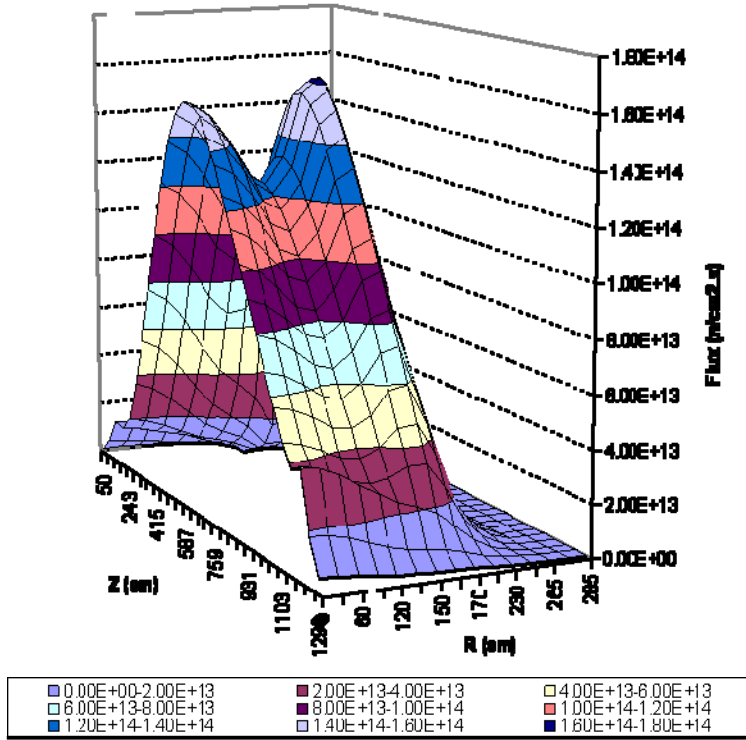


Figure 6. Case 1 thermal flux (n/cm².s).

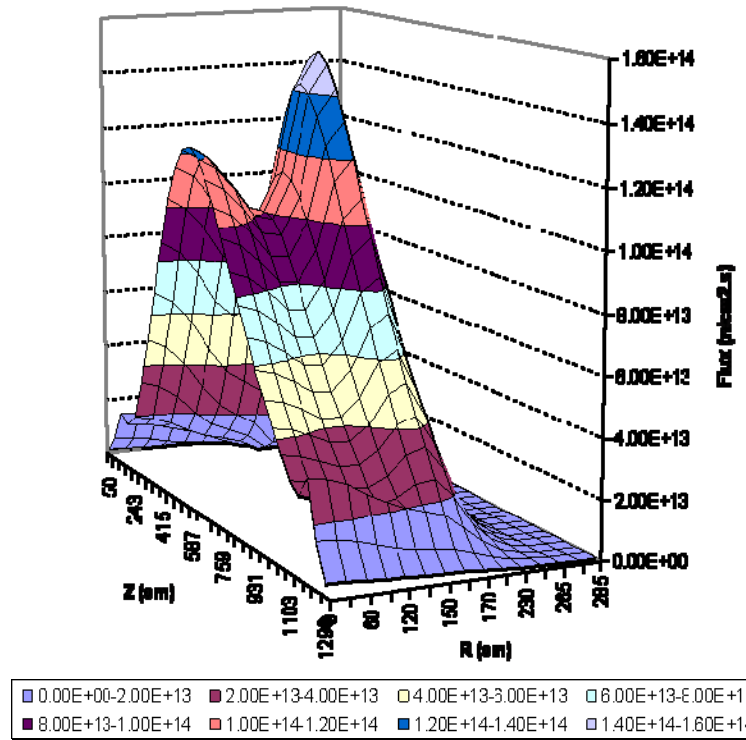


Figure 7. Case 2 thermal flux (n/cm².s).

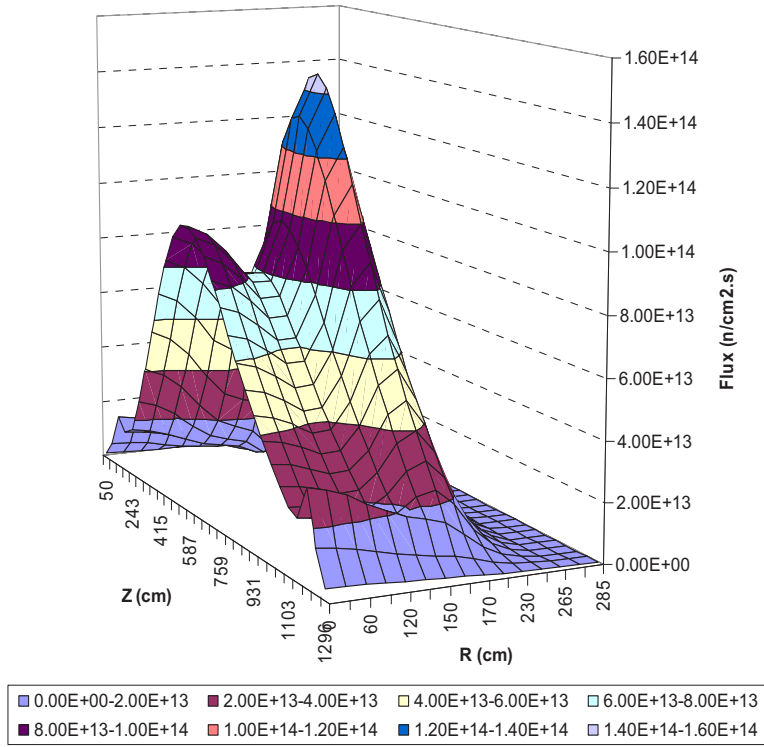


Figure 8. Case 3 thermal flux (n/cm².s).

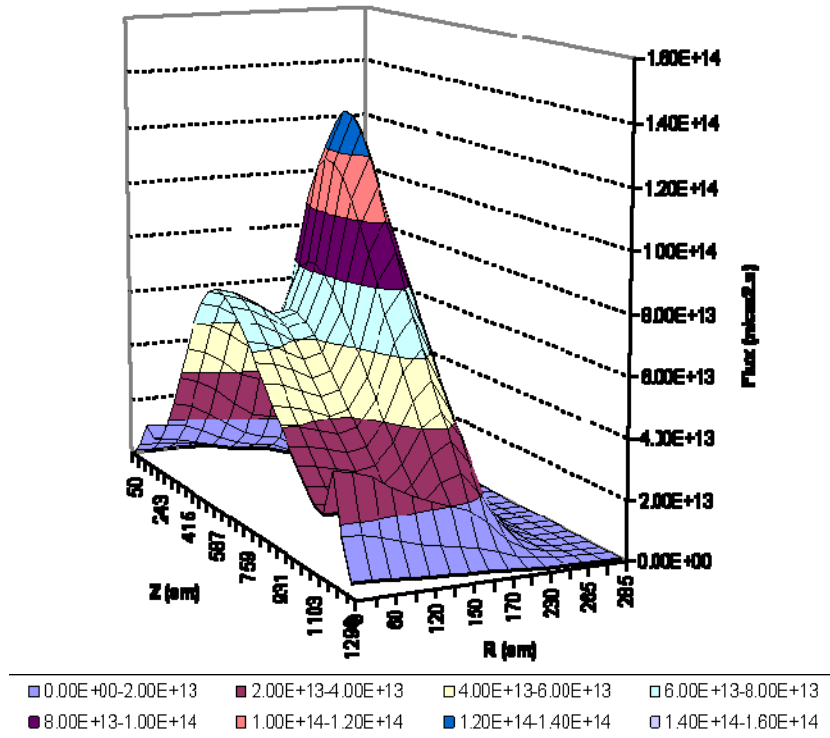


Figure 9. Case 4 thermal flux (n/cm².s).

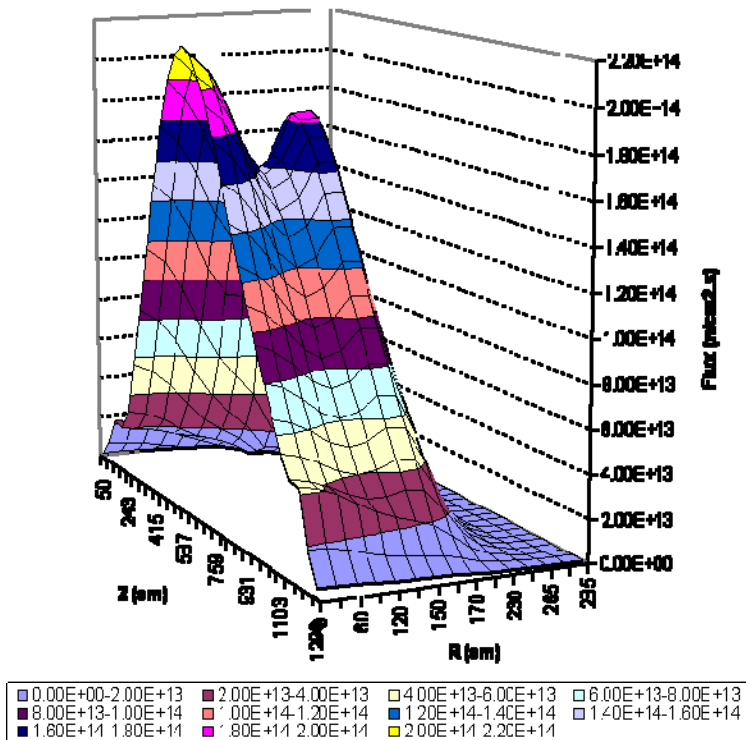


Figure 10. Case 5 thermal flux (n/cm².s).

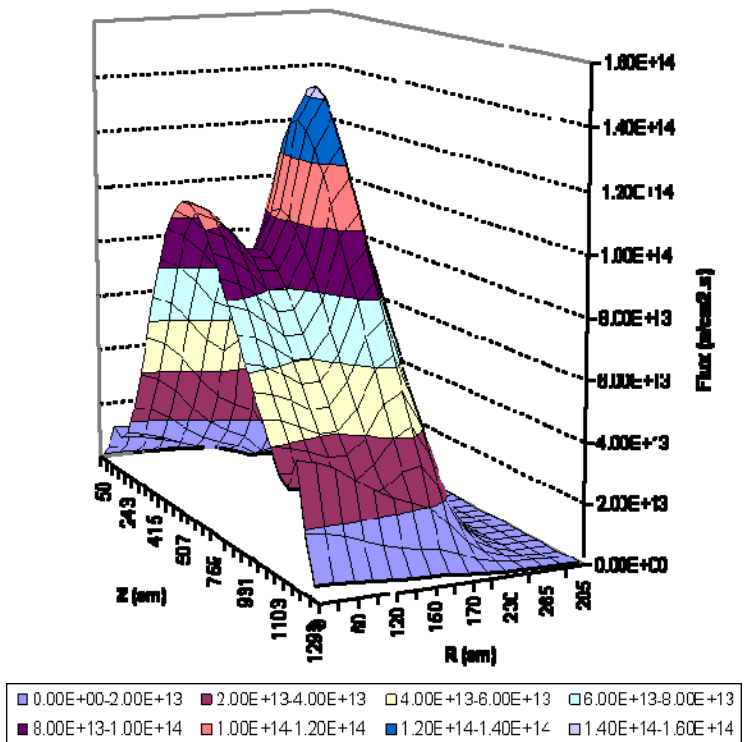


Figure 11. Case 6 thermal flux (n/cm².s).

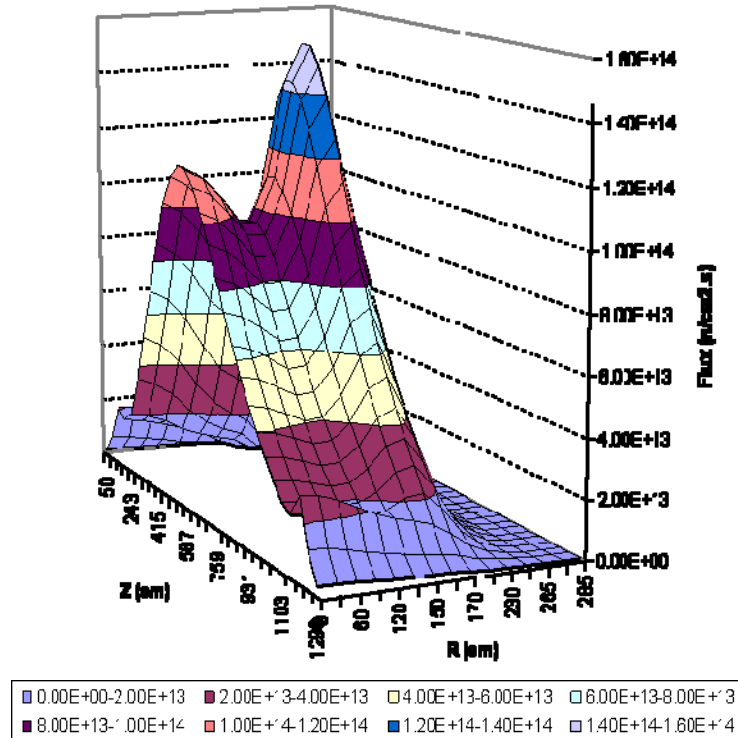


Figure 12. Case 7 thermal flux (n/cm².s).

3.2.2 Power Density Comparisons

The power density for Cases 1–7 are shown in Figure 13 through Figure 19. Two examples of radial and axial cuts are also included at specific locations (Figure 20 and Figure 21). Since the power density is basically a normalized reaction rate, the observed trends closely follow the flux data discussed in Section 3.2.1, which is the combined result of the spatial fast and thermal fluxes. If the Case 1 fast flux shape (Figure 4) is merged with the thermal flux shape (Figure 6) and normalized to a reaction rate that equals 200 MW, the power density shape shown in Figure 13 can be obtained. Since no new insights are obtained from the power density data in this aspect, the data in this section is presented without further discussion.

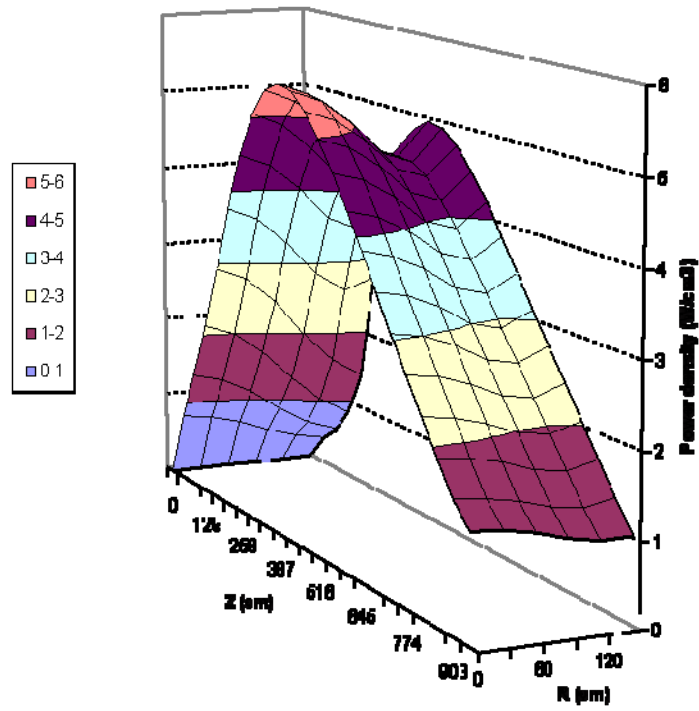


Figure 13. Case 1 power density (W/cm^3).

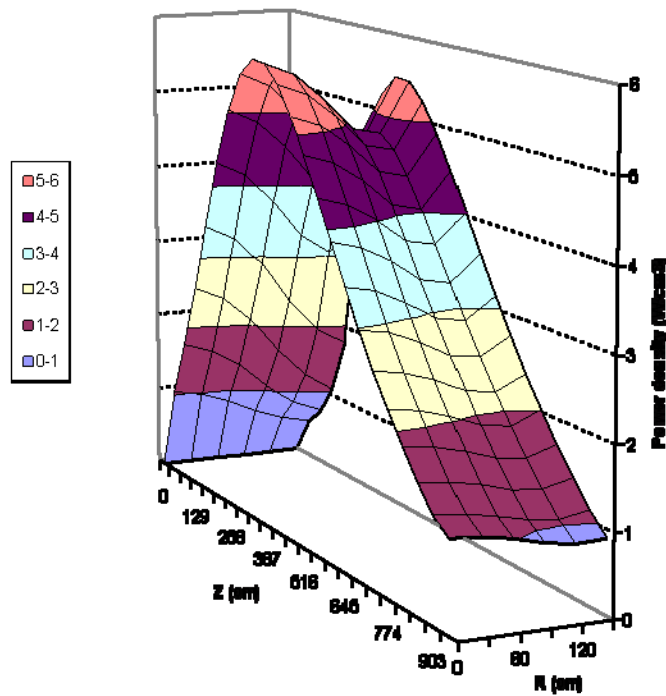


Figure 14. Case 2 power density (W/cm^3).

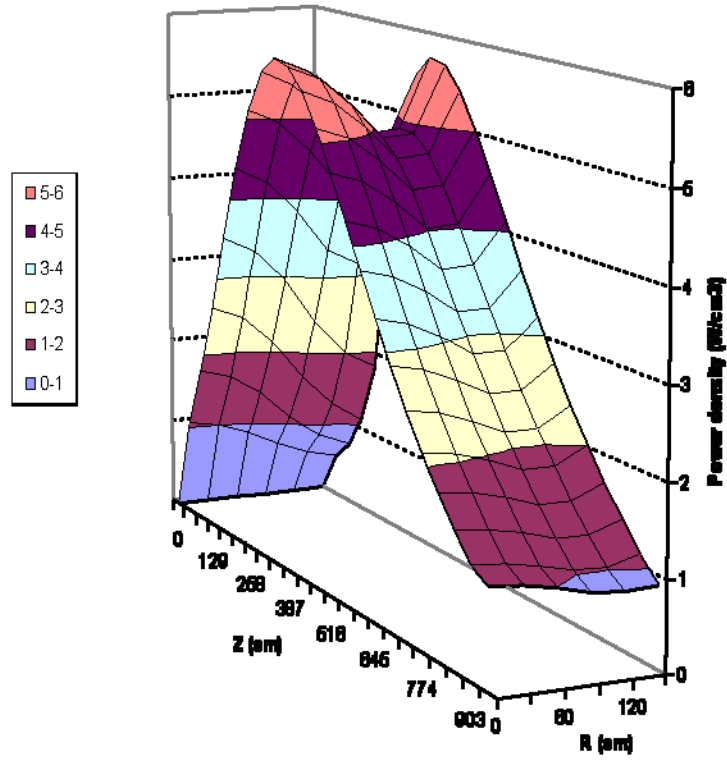


Figure 15. Case 3 power density (W/cm^3).

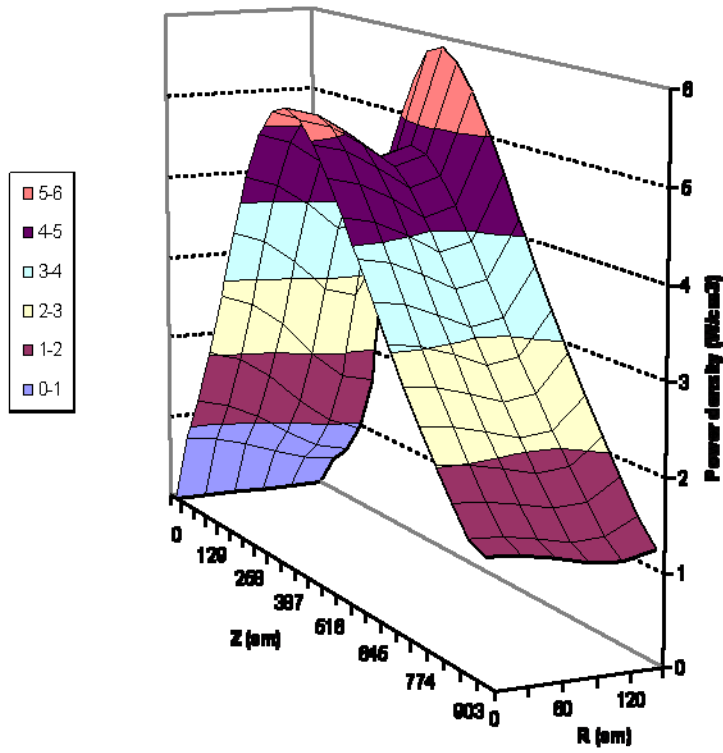


Figure 16. Case 4 power density (W/cm^3).

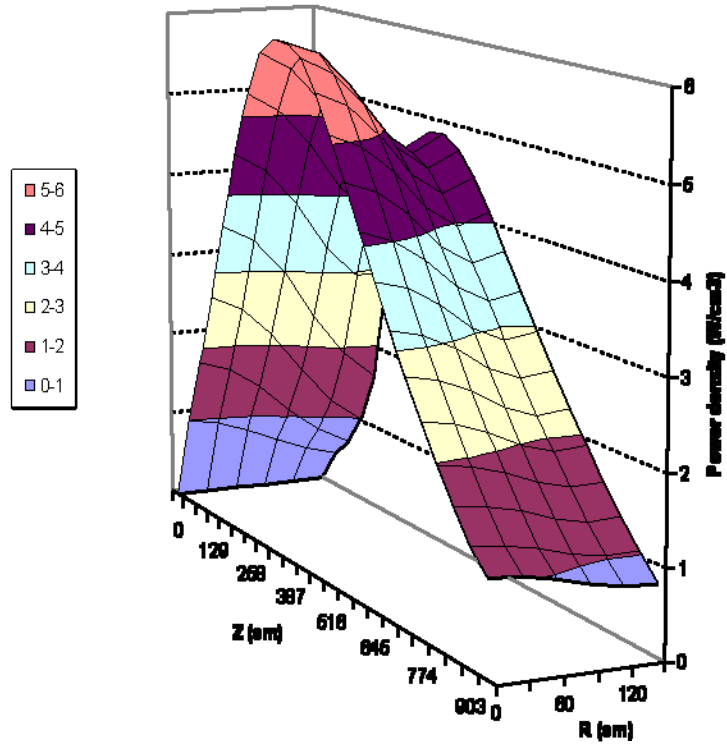


Figure 17. Case 5 power density (W/cm³).

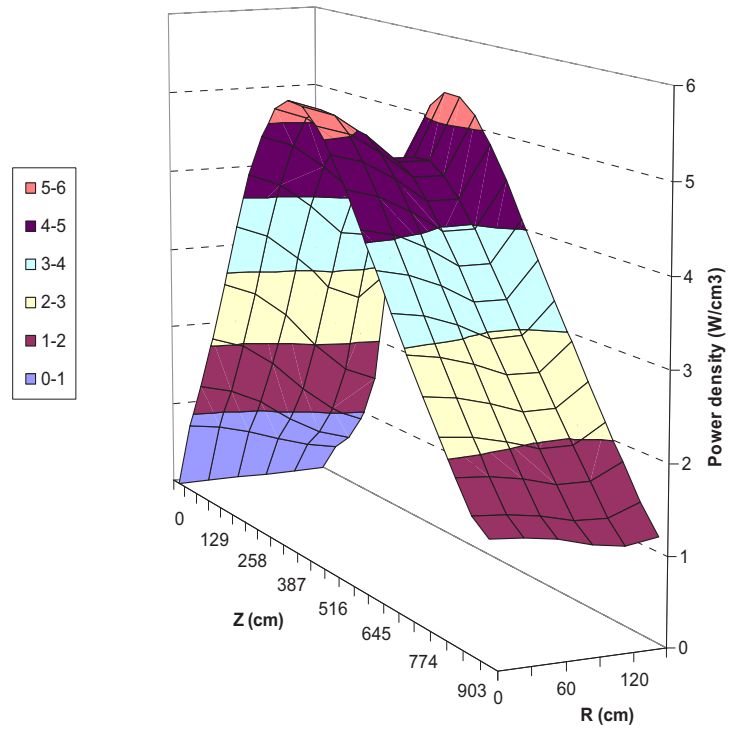


Figure 18. Case 6 power density (W/cm³).

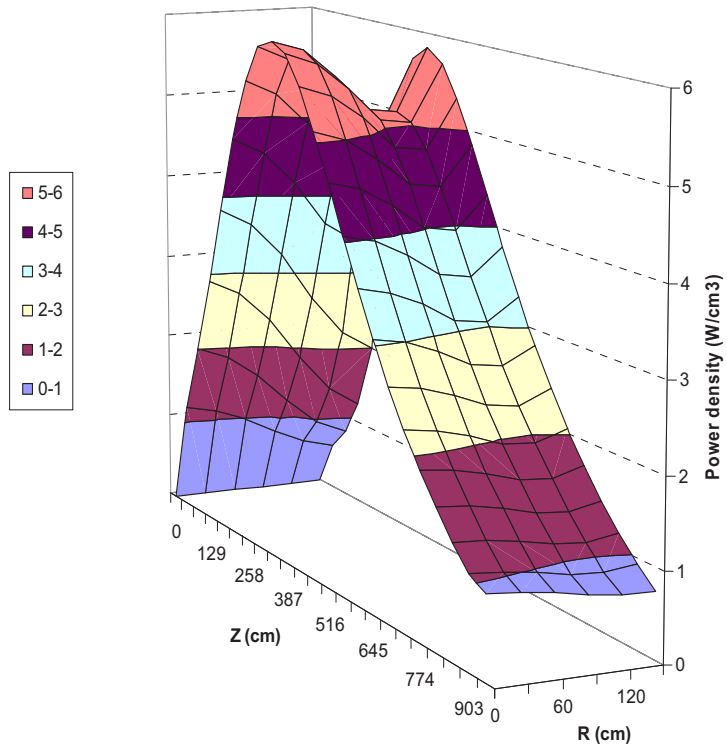


Figure 19. Case 7 power density (W/cm^3).

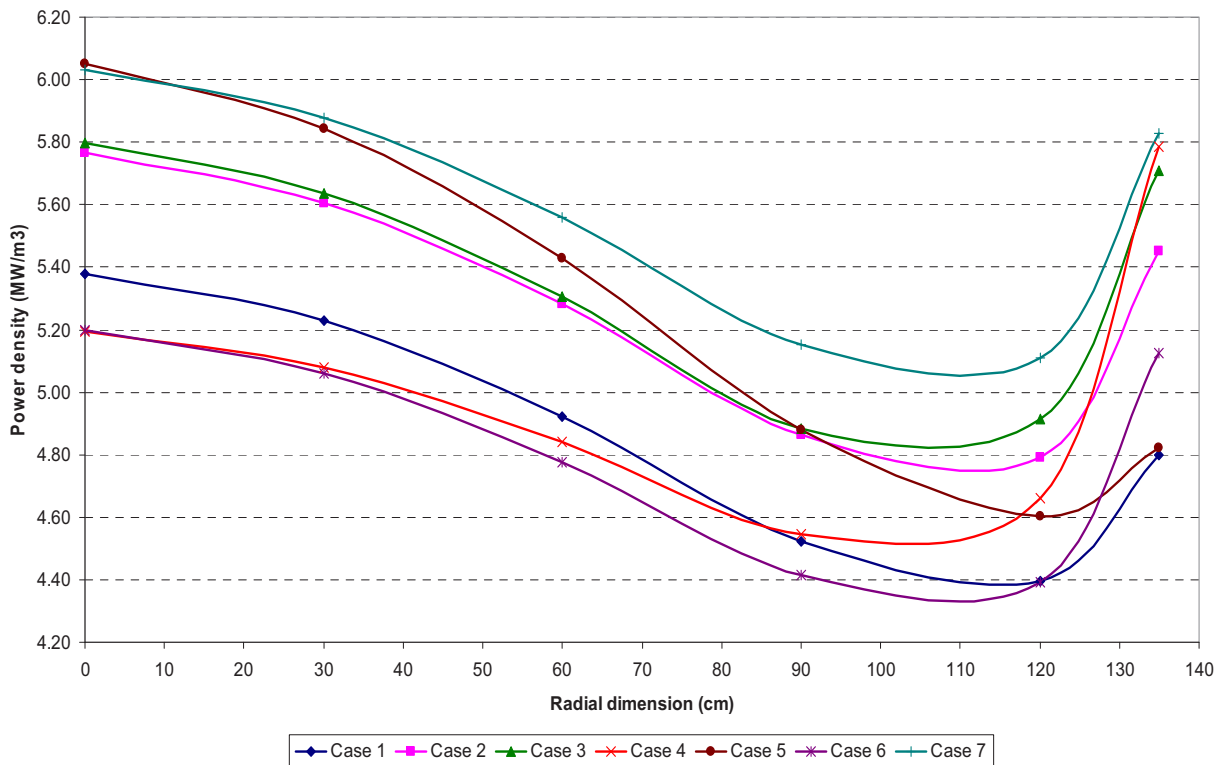


Figure 20. Cases 1–7 radial power density (MW/m^3) at $z = 344$ cm.

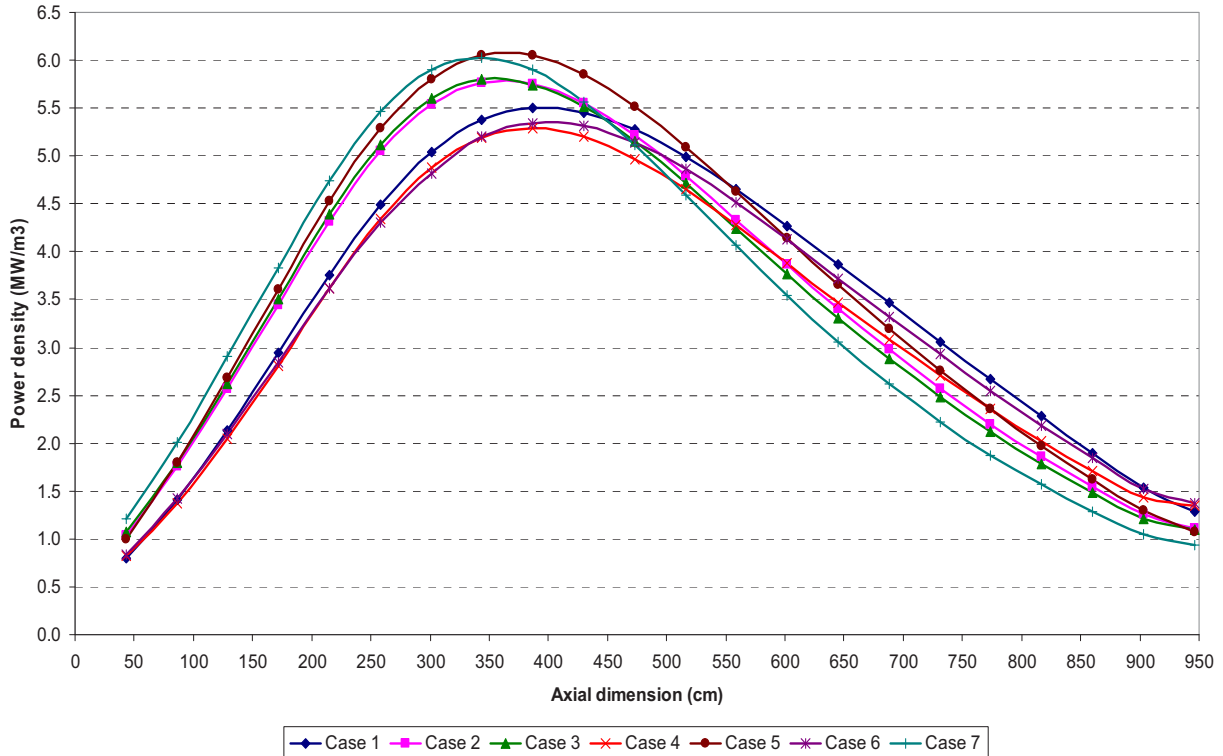


Figure 21. Cases 1–7 axial power density (MW/m³) at r = 15 cm.

3.2.3 Temperature Comparisons

The solid temperature maps for Cases 1 and 3 are presented in Figure 22 and Figure 23, as well as two comparisons of the axial (see Figure 24) and radial (see Figure 25) temperature profiles for all seven cases at $r = 7.5$ cm and $z = 450$ cm, respectively. The hottest regions in the maps occur in the bottom region of the core area (indicated with a red rectangle), and into the porous bottom reflector, where the heat from the core is transported downwards to the outlet plenum. The contour maps in Figure 22 and Figure 23 provide an overview of the volumes of fuel and reflector graphite that are experiencing certain temperature intervals, e.g., less than ~20% of the Case 3 core fuel volume have temperatures in the range 750 to 825°C. Since the maps do not vary much between the cases (forced convection during normal operation dominates any differences that might exist during the nonconvective phase discussed in Section 3.3), only two examples are included here.

The axial profiles in Figure 24 all show the typical heat-up to the lower regions of the core, as well as the constant gradients outside the heat generating core region ($z > 940$ cm). The maximum differences between the cases (around 100°C) is reached in the core center regions, i.e., $z = 500$ cm, with Case 1 displaying higher temperatures compared to the UCO Case 3. The drop-off in temperatures outside the core region is even more pronounced in the radial profiles (see Figure 25), but in this case, the sharp nonlinear gradients are caused by the 10% core bypass cold gas that flows downwards in the control rod channel at $r = 170$ cm.

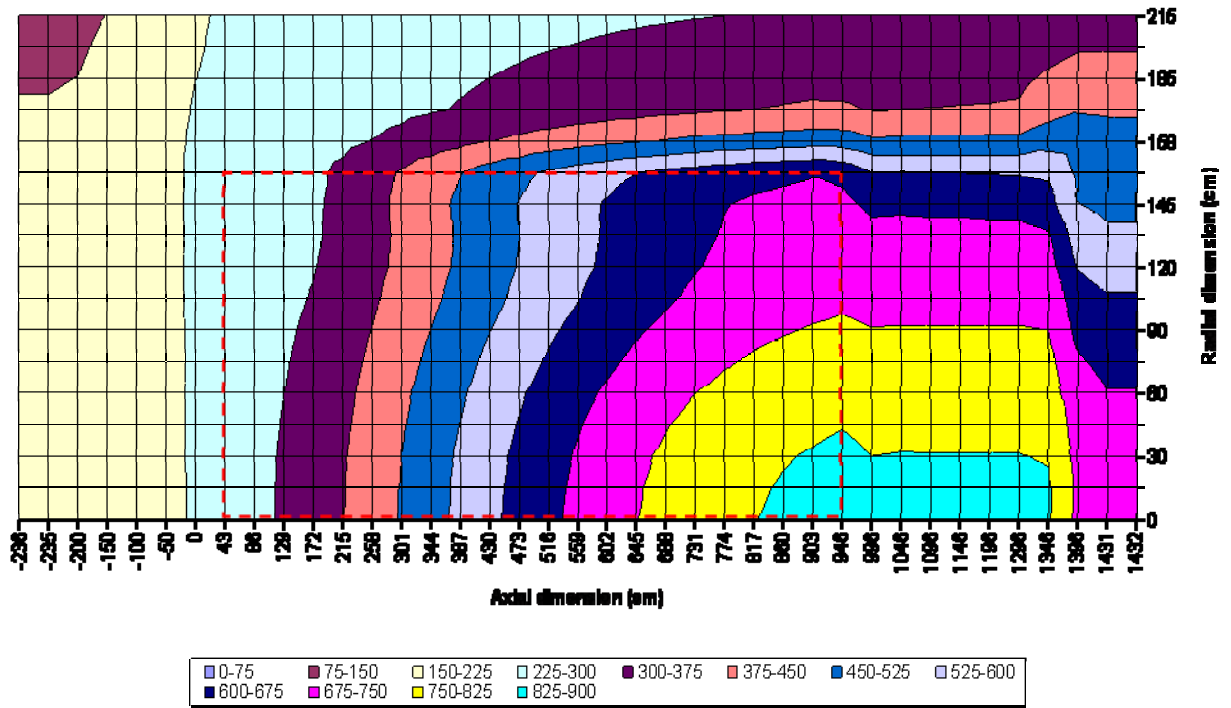


Figure 22. Case 1 solid material temperature (°C) – 2-D contour plot.

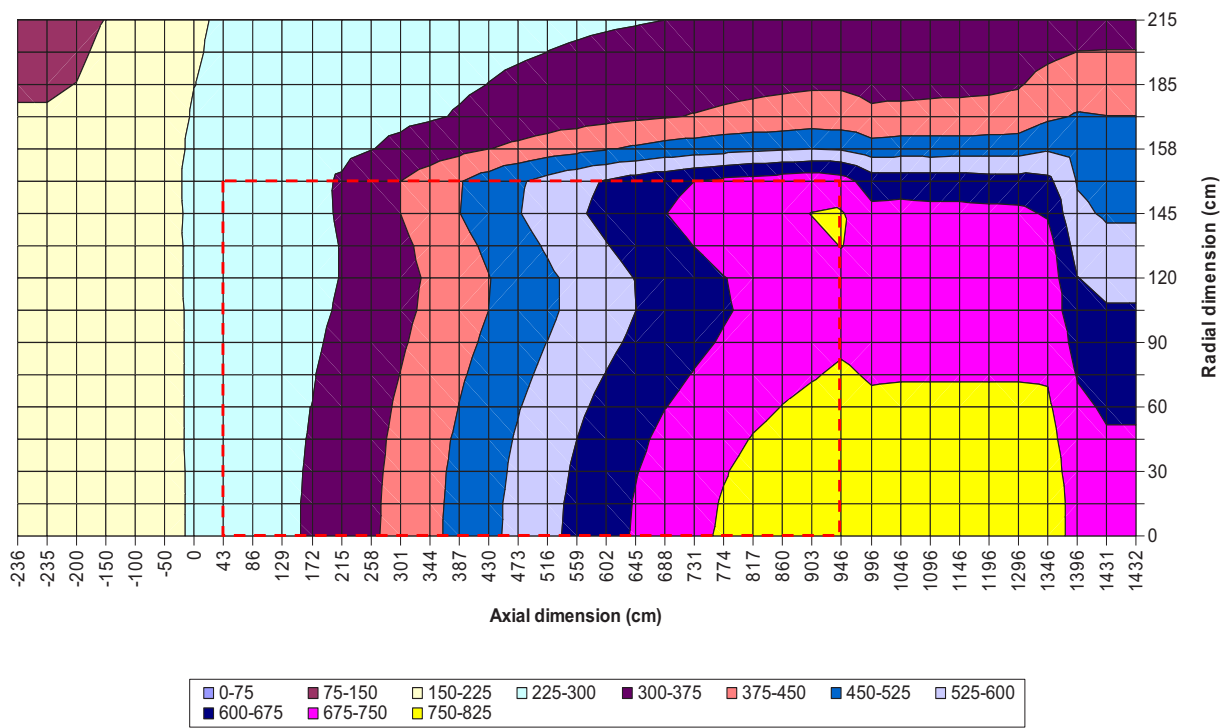


Figure 23. Case 3 solid material temperature (°C) – 2-D contour plot.

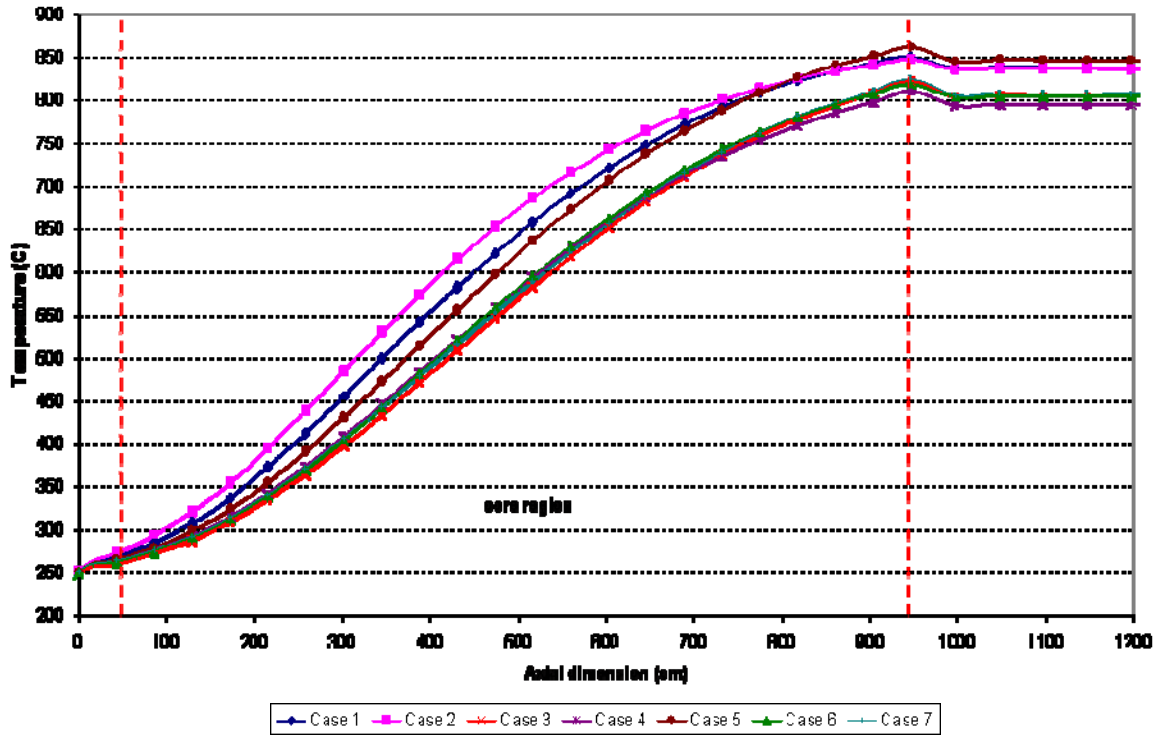


Figure 24. Cases 1–6 axial solid material temperature (°C) at $r = 7.5$ cm.

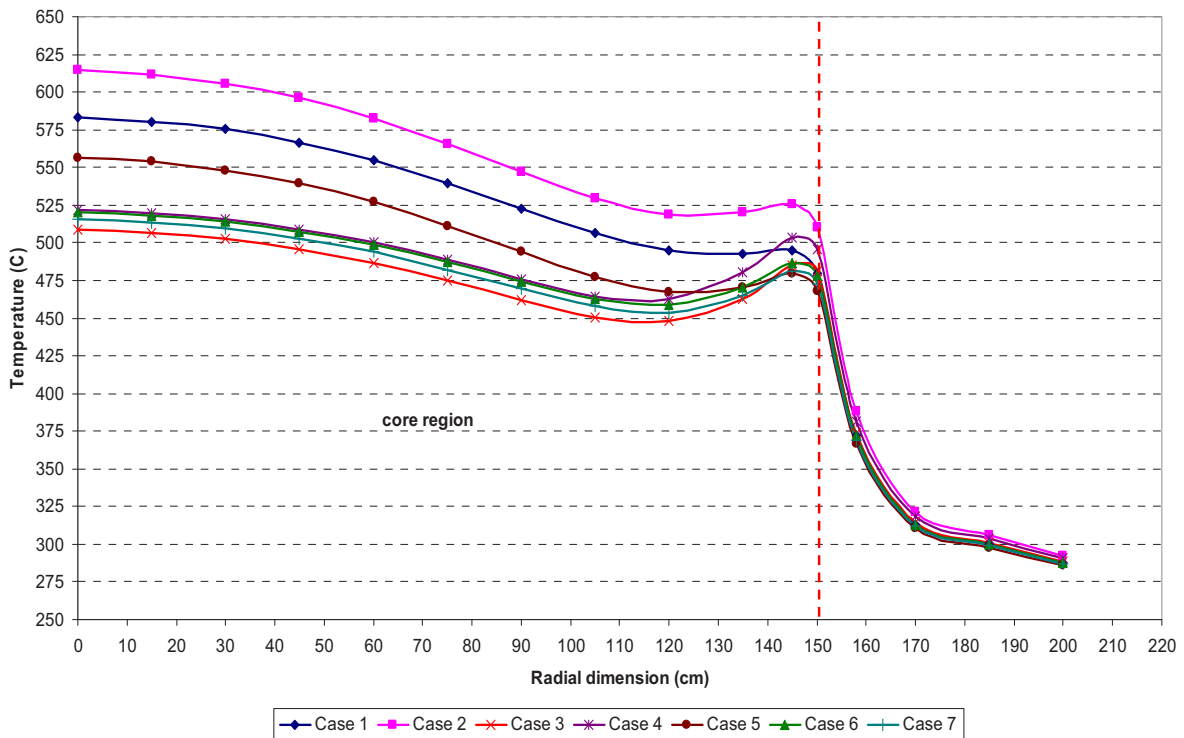


Figure 25. Cases 1–6 radial solid material temperature (°C) at $z = 450$ cm.

A final temperature comparison is shown in Figure 26, where the fuel shell temperatures for the seven cases are compared at a fixed location in the core region ($r = 7.5$ cm, $z = 451$ cm). The PEBBED fuel temperature model consists of a 1-D conduction calculation performed over five thin shells within a representative fuel sphere at a specific core location. Table 5 shows the same data at the five concentric shells radii in the fuel sphere models, as well as the total temperature gradient over the fuel spheres (i.e., the center temperature minus the surface temperature). In spite of large differences between the fuel surface and center temperatures (e.g., between Case 1 and 3 as large as 14% on the surface) of the seven cases, the resultant temperature gradient over the fuel only differs by about 7°C. This can be attributed to the small differences that exist in the power generation per sphere (see Table 4 above for details).

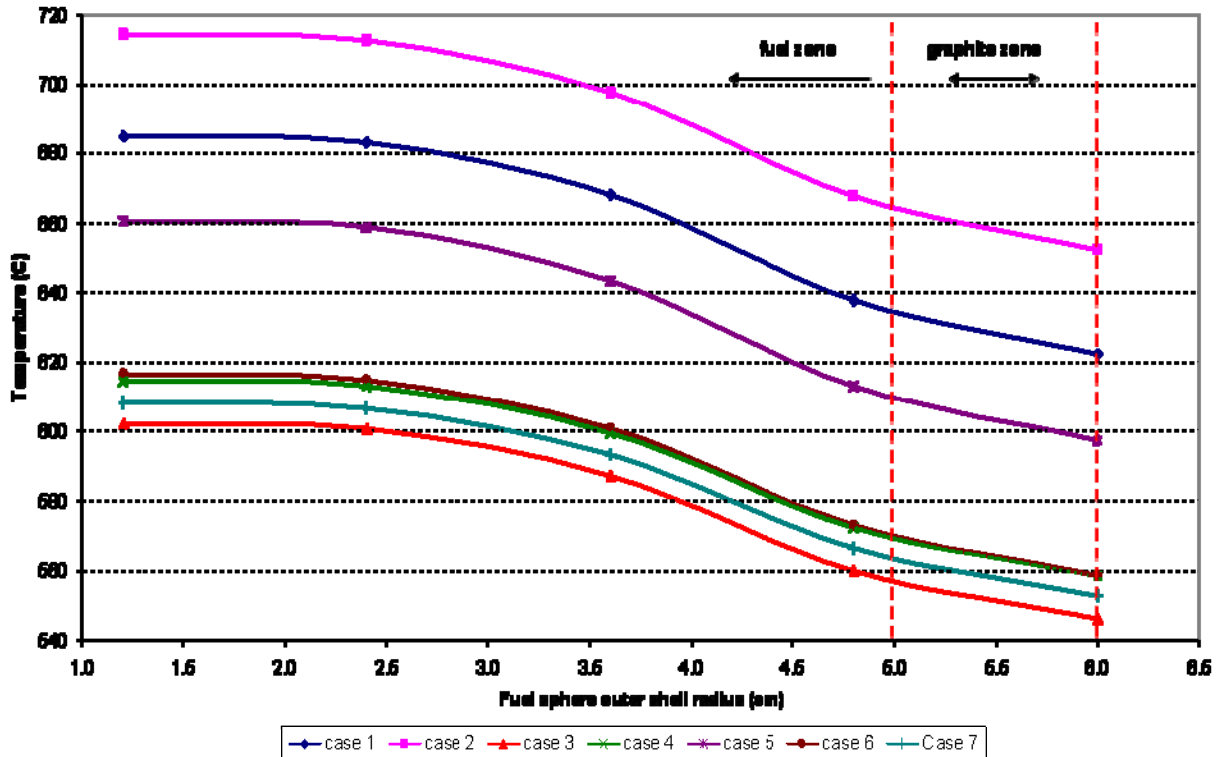


Figure 26. Fuel sphere shell temperatures (°C) at core location ($r; z$) = (7.5 cm; 451 cm).

Table 5. Fuel sphere shell temperatures (°C) at core location ($r; z$) = (7.5 cm; 451 cm).

Fuel shell edge (cm)	Case 1	Case 2	Case 3	Case 4	Case 5	Case 6	Case 7
6.0	623	652	546	559	597	559	553
4.8	638	668	560	572	613	573	567
3.6	668	698	587	599	644	601	593
2.4	683	713	601	613	659	615	607
1.2	685	715	602	615	661	617	608
Gradient over sphere	63	62	56	56	63	58	56

3.2.4 Control Rod Worth Comparisons

Table 6 presents the results of the control rod worth comparison for Cases 1–7. The total control rod worth (expressed as % delta k/k) was determined by subtracting the k-eff value of the fully inserted control rod bank from the k-eff value of the control rods at their nominal location (172 cm below the bottom of the top reflector). The HTR module control rods were not designed to cover the full length of the core, and the maximum insertion depth was limited to 680 cm. (In the PEBBED model a depth of 688 cm was used because of the axial coarse mesh sizes). This shutdown worth is an indication of the available margin at operational conditions, if a SCRAM or controlled insertion should be performed. As a rough guideline, an additional 1% margin is usually required (accounting for uncertainties), i.e., the fully inserted reactivity should counter the core excess reactivity at any time and for any design basis accident, plus 1%.

It can be seen from Table 6 that all the total worths are larger than 4.5%, i.e., 3.5% above the usual required shutdown margin. Case 3, with UCO fuel, therefore has a lower shutdown margin than the UO₂ fueled Case 1, but still well within acceptable limits from a core design point of view. The largest worths in the set is obtained for Case 2, where the change in enrichment resulted in a large thermal flux peak in the side reflector, and Case 5, where the 5 g heavy metal loading lead to beneficial changes in the thermal spectrum and the moderation ratio.

The last line entries in Table 6 are the reactivity additions that occur when a full control rod bank withdrawal is performed. Because of the large thermal flux peak in the side reflector for Case 3 (see Figure 8), the UCO Case 3 has a significantly higher reactivity insertion compared to Case 1. The effect of these withdrawals on the maximum fuel temperatures and total core power can only be estimated with a coupled transient code such as CYNOD-THERMIX, and cannot be provided as part of this study.

Table 6. Cases 1–7 Control Rod Worths.

Description	Case 1	Case 2	Case 3	Case 4	Case 5	Case 6	Case 7
k-eff: CR at nominal position (172 cm)	1.00006	0.99735	0.99999	0.99963	1.00041	1.00025	1.00007
k-eff: All CR fully withdrawn to 0 cm	1.01220	1.01330	1.01487	1.01318	1.01499	1.01360	1.02013
k-eff: All CR fully inserted to 688 cm	0.94411	0.91644	0.95206	0.95427	0.94176	0.95085	0.94643
Total CR worth (% delta k/k)	5.59	8.11	4.79	4.54	5.86	4.94	5.36
Reactivity addition from withdrawal at operating conditions (% delta k/k)	1.21	1.60	1.49	1.36	1.46	1.33	2.01

3.3 DLOFC Results

The DLOFC results for Cases 1–7 are presented in Table 7 and Figure 27. The DLOFC scenario was modeled in PEBBED-THERMIX by assuming an instantaneous termination of all convective heat transport at the start of the transient, i.e., taking only conduction and radiation heat transport into account. The maximum fuel temperature is a function of space (axial/radial location in the 2-D core model) and time (because of the time dependent decay heat generation), and it is used as a safety case indicator for the potential fission product releases during a postulated large break event. As a core design target, a typical value of 1600°C has been used extensively in the past (1, 2, 3, and 7) as a limit on the DLOFC peak fuel temperature (the maximum fuel temperature value in space and time).

Table 7. Cases 1–7 DLOFC results.

Parameter	Case 1	Case 2	Case 3	Case 4	Case 5	Case 6	Case 7
Maximum DLOFC temperature (°C)	1485	1532	1533	1492	1533	1480	1573
Time point when peak fuel temperature is reached (h)	25.2	26.2	26.2	27.8	24.8	25.8	25.8
Duration of maximum fuel temperature above 1400°C (h)	60	82	82	64	81	58	~100

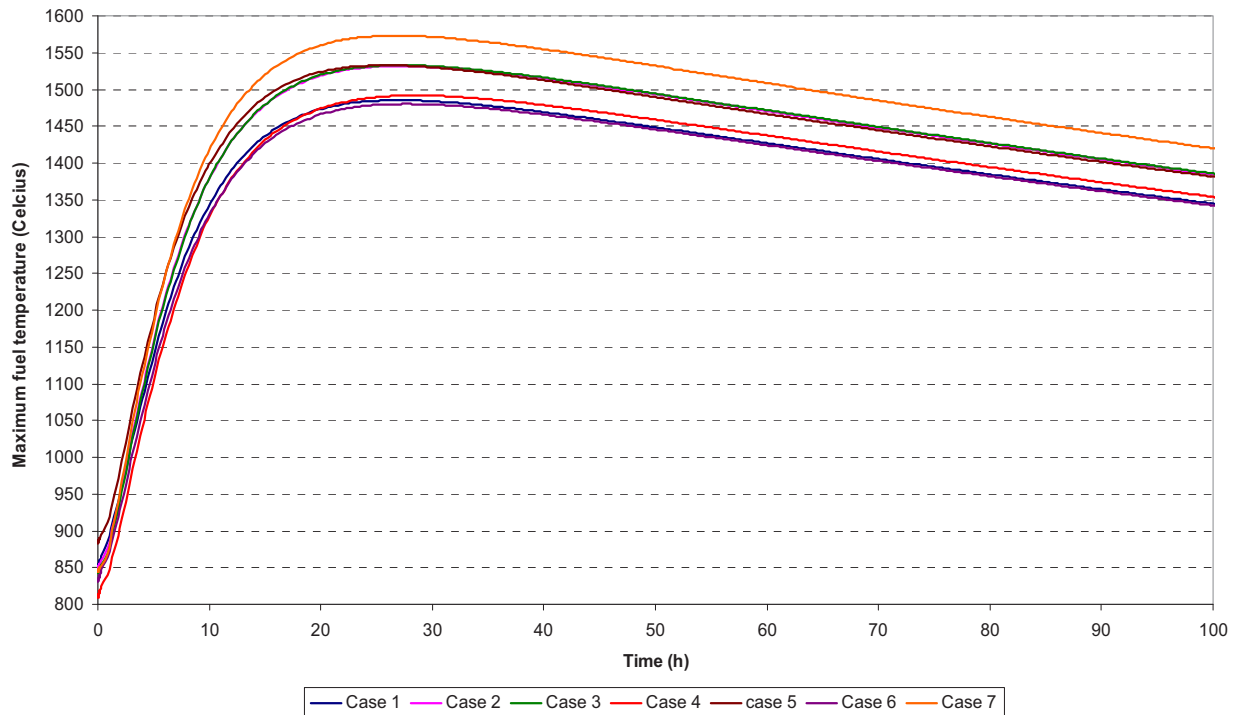


Figure 27. Cases 1–6 DLOFC maximum fuel temperature (°C) vs. time.

In a safety case context, it needs to be demonstrated that the fuel temperatures stay below this limit, even when uncertainties are taken into account. With the exception of the zero graphite fluence assumption (which lead to optimistic results), all results in this study are best estimates. Previous studies indicate that the inclusion of the main uncertainty contributors (decay heat, thermal conductivity, etc.) lead to uncertainty estimates of $2\sigma = \pm 4\%$ ¹³ to $2\sigma = \pm 7\%$.¹² The following observations can be made from the data in Table 7:

- The PEBBED best estimate peak fuel temperature for Case 1 (1485°C) are well below 1600°C, which compares well with the published HTR module results.¹ (The *Pebble Bed Modular Reactor Proprietary HTR Module Safety Analysis Report* includes more detailed results, but it cannot be referenced in the public domain). The HTR module result included some conservative parameters (using 105% power, 8% additional decay heat, bypass flows of 5%, etc.), which combined, using the Sum of the Root Squares (SRS) method, produced a conservative peak fuel temperature estimate of 1550°C (this included the margin of 70°C). If a margin of 4% (59°C) to 7% (104°C) is added to the PEBBED best estimate result, the conservative peak fuel temperature estimate for Case 1 ranges between 1544 and 1589°C, which is comparable to the HTR module result of 1550°C, yet still below 1600°C.

- The peak DLOFC fuel temperature is reached between 25 and 28 hours into the transient, and the durations that the hottest fuel spends above 1400°C vary between 60 to over 100 hours (Figure 28). The data in Table 8 shows that only small volumes of the fuel (approximately 4% of the 360,000 spheres) experience these elevated temperatures. The fuel-volume distribution in various temperature intervals are shown in Figure 29, and for all seven cases, more than 54% of the fuel had a maximum fuel temperature below 1000°C. These snapshots were taken at the time when the peak fuel temperature occurs for each case.

Table 8. Cases 1–7 maximum fuel temperature volumetric distribution (% of total fuel volume).

Temperature Interval (°C)	Case 1	Case 2	Case 3	Case 4	Case 5	Case 6	Case 7
<1000	62	67	68	62	67	62	54
1000–1200	26	11	12	25	12	26	26
1200–1400	8	18	16	8	18	8	16
1400–1600	4	4	4	4	4	4	4

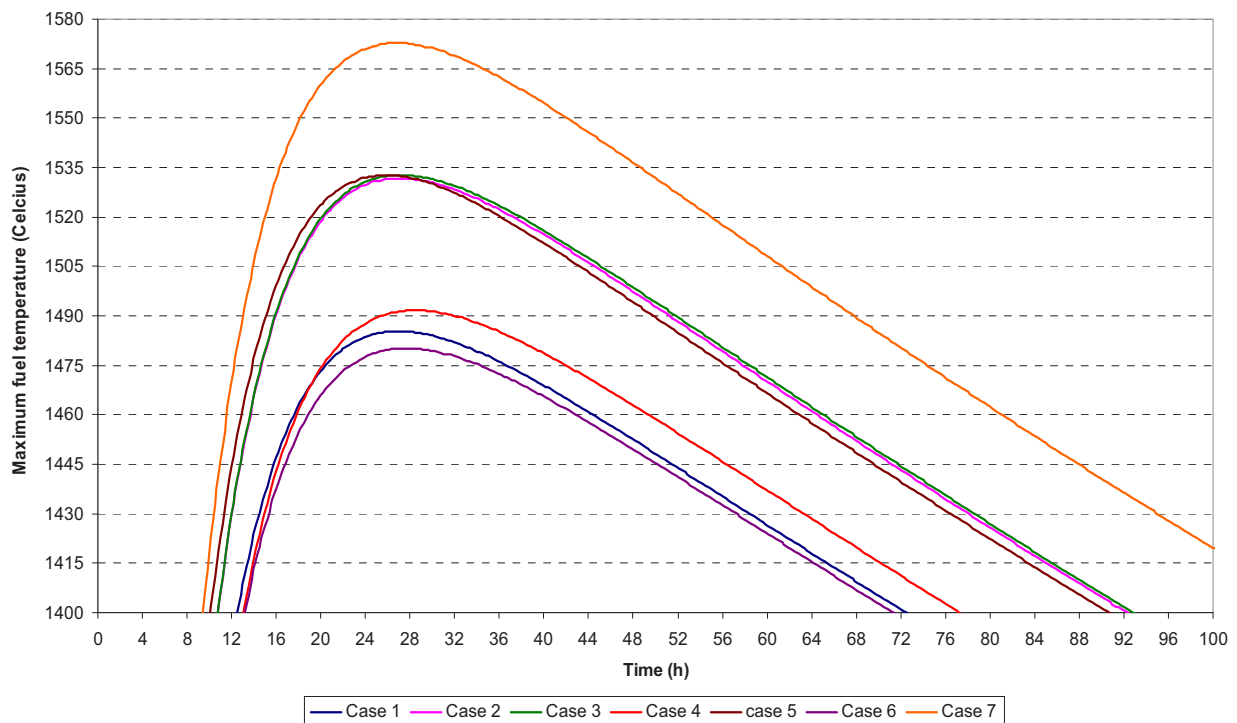


Figure 28. Cases 1–6 DLOFC maximum fuel temperature (°C) vs. time – detail of the time spent above 1400°C.

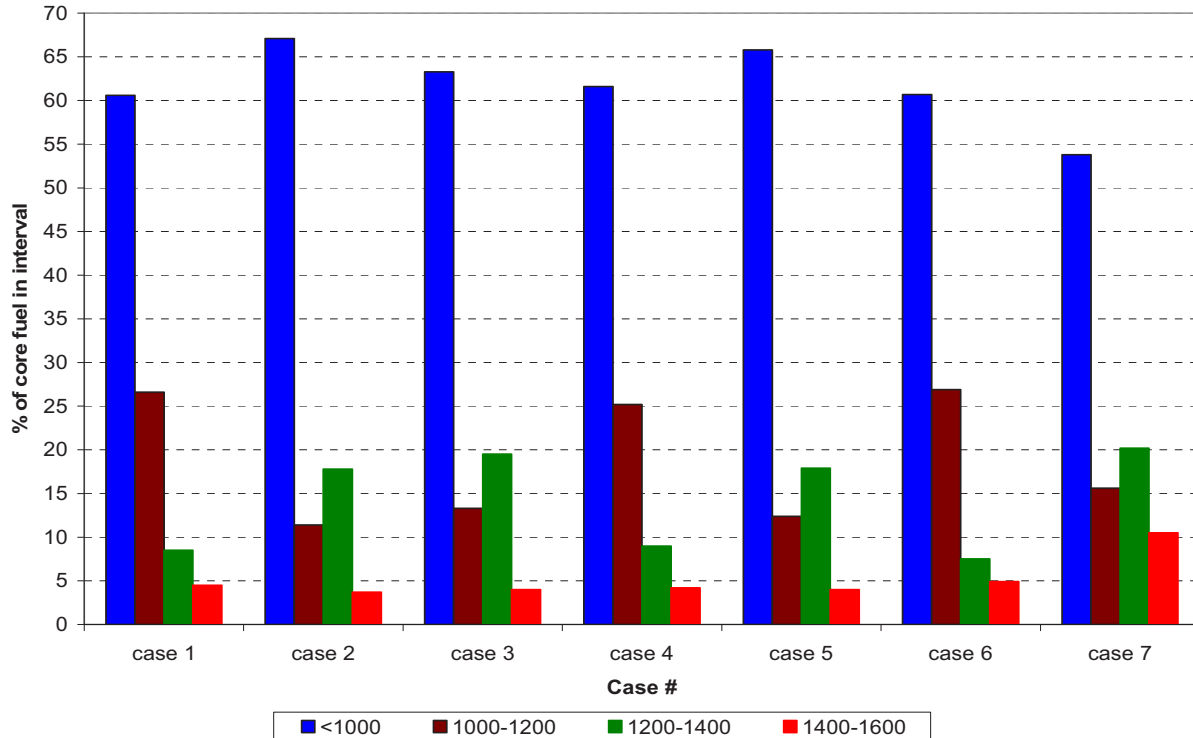


Figure 29. Cases 1–7 maximum fuel temperature volumetric distribution (% of total fuel volume).

- The use of UCO fuel at 14% enriched and 150 MWd/kg U burnup (Case 3) lead to a small increase of 48°C (3%) in the DLOFC peak fuel temperature. This is caused by the combined effect of the upwards-shifted axial power profile (Figure 21), and the upwards movement of heat through conduction and radiation in the core. (The main heat loss path for the decay heat in the core during a DLOFC is upwards, since the bottom of the core is hotter than the upper areas during normal operation, and outwards in the radial direction through the side reflector). Changes in the steady-state power profiles (e.g., as shown in Figure 15, Figure 20, and Figure 21) are responsible for most of the differences that exist between these cases, since these power shapes also represent the DLOFC decay heat generation distribution. This effect can be best seen for Case 7, where the decrease to 10 fuel passes resulted in a large upwards shift in the axial profile (Figure 21), and a significant tilt towards the radial center of the core in the radial power profile (Figure 19).
- The DLOFC data for Case 2 and 3 are essentially identical, indicating that the change from UO₂ to UCO fuel kernels is not the determining factor for the DLOFC fuel temperatures, but rather the change in enrichment and the resultant higher burnup achieved.
- A peak fuel temperature difference of 41°C is observed between the 9 and 5 grams heavy metal loading of Cases 4 and 5, with the lower heavy metal loading leading to the higher DLOFC fuel temperature. As indicated in Section 3.2, the lower number of UCO particles (13,550) loaded per fuel sphere in Case 5 still need to produce the same total power as the 26,650 UCO particles loaded in Case 4. The Case 5 fuel will therefore have a higher decay heat production per sphere, and combined with shift in the axial and radial power profiles, these two effects lead to the increase in peak fuel temperature.
- Only Case 7 (1573°C) produced peak fuel temperatures in excess of 1550°C because of the reduction to 10 fuel passes through the core. If the uncertainty margins are added to these results, a 10 pass operational regime would probably be too close to the acceptable fuel temperature margins. The data

in Table 7 indicates that an increase of five passes on average could be worth around 40 to 60°C in the peak DLOFC fuel temperature. An increase in the number of passes is an effective core design method to decrease the DLOFC temperatures (as well as the core axial height, cooling the reflector, and, to a lesser degree, the core radius), but it has significant fuel handling cost implications that need to be included in a core optimization study.

3.4 Water Ingress Results

For the HTR module design, the heavy metal loading selected was such that accidental water ingress into the primary system resulted in a lower reactivity increase than is caused by the inadvertent withdrawal of all the reflector rods¹ (the module safety case wanted to present the control rod withdrawal case as the bounding reactivity insertion scenario). From a core design point of view, a lower heavy metal loading is beneficial to reactivity insertion behavior, but it leads to higher fuel costs per kWh produced. The need for a lower heavy metal loading must also be balanced against the power generation per kernel and DLOFC temperature requirements, since a lower heavy metal loading leads to higher power density generated per pebble and a higher DLOFC fuel temperature (see Table 7). For the change to higher enriched UCO fuel, the water ingress event is therefore one of the crucial check that needs to be performed as part of the reactor physics assessment.

In this section, the reactivity addition of the module design will be compared for the UO₂ reference design, the UO₂ fueled core at 14% enrichment, and the five UCO-fueled cases. In a safety report context, water ingress needs to be assessed for three core states: cold shutdown (50°C), hot standby (300°C), and operational. But for this study only, the operational core state will be analyzed. Note that the cold shutdown scenario is actually the bounding reactivity insertion case here, but since the fuel is cold and the core subcritical, the fuel temperature increase is well below operational temperatures. The hot, critical core state produces a smaller reactivity insertion, but it is the bounding case for the fuel temperatures.

The volume of water (in the form of steam) that can enter the primary system is limited by physical constraints. Previous HTR module studies^{1,14} indicated a theoretical limit of 17 tons, which assumes a primary system fully saturated with steam at 7 MPa and 270°C, and no helium present. However, since this is not a realistic or even probable scenario, the design basis accident for the HTR module only considered the ingress of 600 kg water into the primary system. For this study, the reactivity behavior is shown up to 6,600 kg to illustrate the turn-around point above which additional steam ingress only decreases reactivity.

The water ingress results for Cases 1–7 are presented in Figure 30 and Table 9. The calculated trends for all the cases are typical of under-moderated systems, i.e., an increase in reactivity followed by a phase where additional water acts as a neutron poison. Case 5, with a lower heavy metal loading (5 grams), is close to the point where water ingress becomes a nonissue from a reactivity point of view (graphite corrosion would, however, still be an issue), since only a very small reactivity increase of 0.04% (40 pcm) is observed at 330 kg steam (Table 9). On the other end of the spectrum is the 9 gram heavy metal loading Case 4, which reaches a peak reactivity insertion value of 5.05% (5,050 pcm) after 5,280 kg of steam has been added to the core volume. This is almost three times higher than the reference HTR module Case 1 peak value of 1.63% at 1,980 kg.

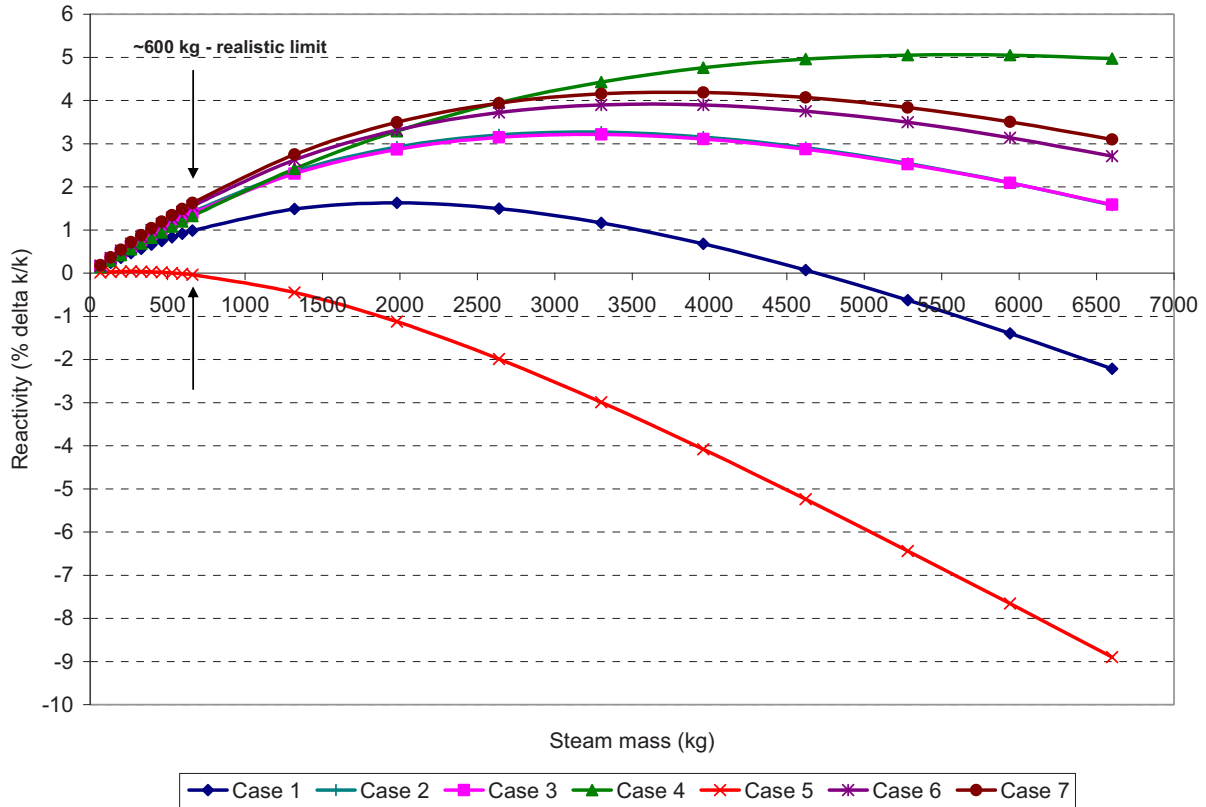


Figure 30. Cases 1–6 reactivity addition (%) because of water ingress (kg).

Table 9. Cases 1–7 water ingress results.

Steam Density g/cc	Steam Mass kg	Reactivity change (% delta k/k)						
		Case 1	Case 2	Case 3	Case 4	Case 5	Case 6	Case 7
0.001	66	0.12	0.17	0.16	0.14	0.01	0.18	0.19
0.002	132	0.24	0.33	0.32	0.28	0.03	0.35	0.37
0.003	198	0.36	0.48	0.47	0.42	0.03	0.52	0.55
0.004	264	0.46	0.63	0.62	0.55	0.04	0.69	0.72
0.005	330	0.56	0.78	0.76	0.69	0.04	0.84	0.88
0.006	396	0.66	0.92	0.90	0.82	0.03	1.00	1.04
0.007	462	0.75	1.05	1.03	0.95	0.02	1.14	1.20
0.008	528	0.83	1.18	1.15	1.08	0.01	1.29	1.34
0.009	594	0.91	1.30	1.27	1.20	-0.01	1.42	1.49
0.010	660	0.99	1.42	1.39	1.32	-0.03	1.55	1.63
0.020	1320	1.48	2.36	2.31	2.42	-0.45	2.62	2.75
0.030	1980	1.63	2.92	2.86	3.29	-1.13	3.32	3.49
0.040	2640	1.50	3.21	3.15	3.95	-1.99	3.72	3.94
0.050	3300	1.17	3.27	3.21	4.43	-2.99	3.90	4.16
0.060	3960	0.68	3.16	3.11	4.76	-4.08	3.90	4.19
0.070	4620	0.07	2.91	2.87	4.96	-5.24	3.75	4.07
0.080	5280	-0.63	2.55	2.53	5.05	-6.44	3.49	3.84
0.090	5940	-1.39	2.10	2.09	5.05	-7.66	3.14	3.51
0.100	6600	-2.21	1.58	1.59	4.97	-8.90	2.71	3.10

The main focus of this study is the conclusions that can be made from Cases 1, 2, and 3:

- The reactivity behavior of the UO_2 (peak value 1.63% at 1,980 kg) and UCO (3.21% at 3,300 kg) Cases 1 and 3 differ substantially. The UCO fueled core is almost twice as reactive as the UO_2 fueled core for a steam ingress event, and, from a safety point of view, the shutdown capability of these cores must be taken into account. If the control rod worths for a full SCRAM are compared for these two cases (Table 6 gives total worths of 5.6% for Case 1 and 4.8% for Case 3), it can be concluded that an acceptable margin exist for both these cases, although it is less for the UCO fueled core. (The margins for Cases 1 and 3 are 4% and 1.6%, respectively, while an acceptable control rod shutdown margin is usually around 1%). From an accident mitigation point of view, the UCO fuel design therefore leads to a more reactive core, but there is also an adequate reserve shutdown margin available. It therefore seems feasible to operate a HTR module core design with UCO fuel, enriched to 14% and loaded to 7 grams heavy metal. Additional safety margin could be obtained by lowering the heavy metal loading to 6 grams heavy metal per sphere, if desired.
- Since the heavy metal loading of the three cases are identical, changes in the enrichment (from 7.8 to 14%), burnup (89 MWd/kg vs. 165 MWd/kg – see Table 4) and fuel composition (UO_2 vs. UCO kernels) are the only factors that can contribute to the change in reactivity behavior. Case 2 was included in the set specifically to isolate the effect of a higher enrichment on the HTR module UO_2 case. It can be seen in Figure 31 that the reactivity increase of Case 2 accounts for *all* of the increase calculated for Case 3, and that the gradients of Cases 2 and 3 are identical. It can therefore be concluded that the higher enrichment plays the dominant role in the UCO fueled core's reactivity behavior, and not as much in the change to UCO fuel kernels.
- Finally, the reactivity insertion values for 600 kg of steam can be compared with the reactivity added from a full control rod withdrawal, as was done for the HTR module SAR. For Case 1, a full withdrawal lead to an increase of 1.2% (Table 4) vs. 0.99% for the steam ingress, compared with the Case 3 values of 1.5% vs. 1.42%. For both these cases (UO_2 and UCO fueled cores) the control rod withdrawal event is therefore the limiting/bounding case for reactivity insertion, supporting the intent of the original HTR module design.

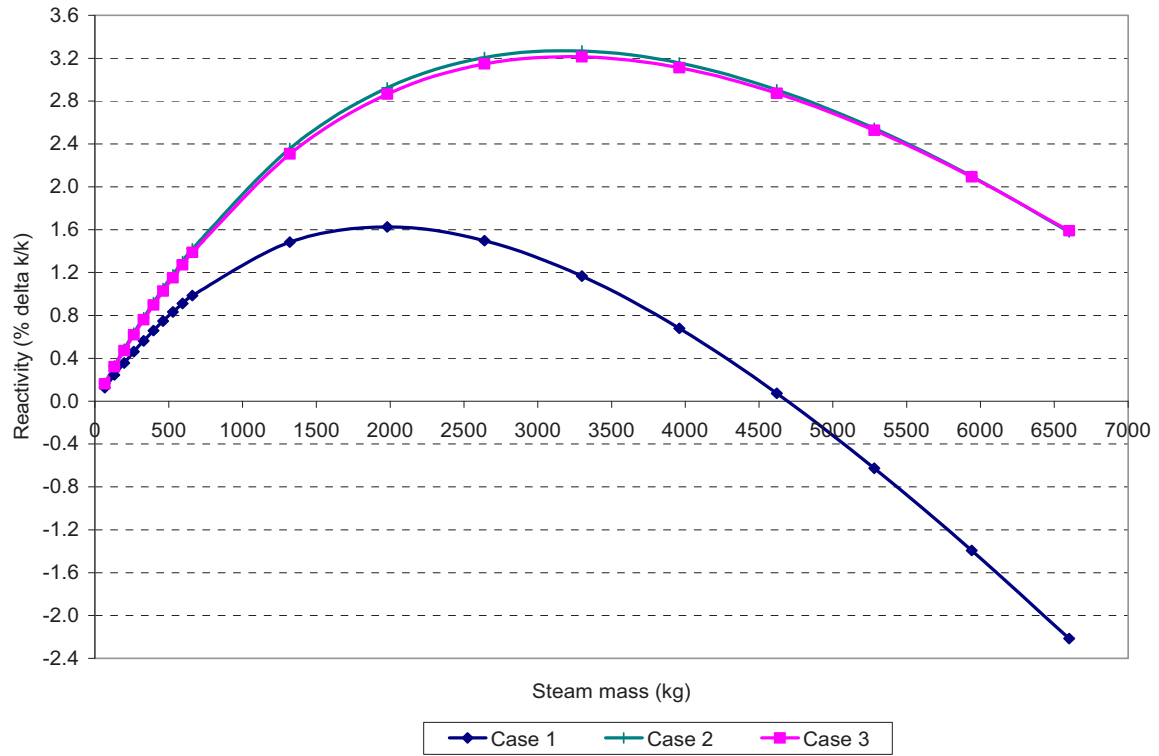


Figure 31. Cases 1–3 reactivity addition (%) because of water ingress (kg).

4. SUMMARY AND CONCLUSIONS

The HTR module design utilized spherical fuel elements packed into a dynamic pebble bed, consisting of TRISO coated uranium oxide (UO₂) fuel kernels with a U-235 enrichment of 7.8% and a heavy metal loading of 7 grams per pebble. The main objective of this study was to compare several important reactor physics and core design parameters for the HTR module and an identical design utilizing UCO fuel kernels. The PEBBED-THERMIX code, which was developed specifically for the analysis of pebble bed HTRs, was used to compare the coupled neutronic and thermal fluid performance of the two designs. Seven cases were developed to answer the following questions:

- *Case 1 and 3:* Can the HTR module be operated with higher enriched UCO fuel to a higher discharge burnup, instead of lower burnt UO₂ fuel, and will it still be within an acceptable safety envelope (reactivity, fuel temperatures, rod worths, etc.)?
- *Case 2:* What is the effect of simply using 14% enrichment on the HTR module with UO₂ fuel? How does this design compare with the 14% enriched HTR module with UCO fuel?
- *Cases 4 and 5:* What is the effect of the heavy metal loading on the operational parameters, and specifically on the water ingress scenario? Is 7 grams heavy metal per sphere still an acceptable choice for the UCO-fueled HTR module, or should a lower loading be considered?
- *Cases 6 and 7:* To what degree can the DLOFC fuel temperatures be influenced by varying the number of fuel passes through the core?

The analysis of the normal operation (steady-state) equilibrium results showed that the dominant contributor to the observed variances between the HTR module UO₂ and UCO cores is the increase in the U-235 enrichment to 14%, and not as much the additional moderation effects of the oxygen to carbon exchange. The flux, power density, and temperature data of Case 2 (where the HTR module was loaded with 14% enriched UO₂ fuel) are very similar to the results of Case 3 (the UCO-fueled core)—certainly within the expected uncertainty margins of these calculations. Although the UCO core displayed higher power densities, it was not carried through to the fuel temperatures, where the differences were found to be minimal.

In addition to the steady-state analyses, two important design basis accidents were also included in this study. The first was an extreme loss of forced cooling accident caused by a large double-ended guillotine break. This event is the limiting case for the fuel temperatures. The second event was the ingress of water (in the form of steam) into the core, because of a hypothetical steam generator tube rupture. The behaviors of the seven core designs were analyzed up to a very conservative 6,600 kg of steam ingress, which yielded the following conclusions:

- The use of UCO fuel at 14% enriched and 150 MWd/kg U burnup (Case 3) lead to a small increase of 48°C (3%) in the DLOFC peak fuel temperature to 1533°C. If typical uncertainty margins between 61°C (4%) and 107°C (7%) are taken into account, the fuel temperatures are still below 1650°C. However, it was also shown that only 4% of the 360,000 fuel spheres in the core have maximum temperatures above 1400°C.
- It was found that the DLOFC fuel temperature data for Cases 2 and 3 are essentially identical; indicating that the determining factor for the DLOFC fuel temperatures is not the change from UO₂ to UCO fuel kernels, but rather, the change in enrichment and the resultant higher burnup achieved.
- For the HTR module design, the heavy metal loading selected was such that an accidental water ingress into the primary system resulted in a lower reactivity increase than is caused by the inadvertent withdrawal of all the reflector rods. The design basis accident for the HTR module only considered the ingress of 600 kg water into the primary system, but for this study, the reactivity behavior was analyzed up to 6,600 kg to illustrate the turn-around point above which additional steam

ingress only decreases reactivity. It was found that the 7 g heavy metal UCO fueled core is almost twice as reactive as the 7 g heavy metal UO_2 fueled core for a steam ingress event (peak value 3.21% at 3,300 kg vs. 1.63% at 1,980 kg). However, the control rod shutdown worths for a full SCRAM were also compared for these two cases (5.6% for Case 1 and 4.8% for Case 3), and it was concluded that an acceptable shutdown margin exists for both cases. It therefore seems feasible, from a water ingress point of view, to operate an HTR module core design with UCO fuel enriched to 14% and loaded to 7 grams heavy metal. A detailed core design optimization could however mitigate or eliminate this under-moderated effect, since the 5g heavy metal Case 5 had almost no reactivity increase, for example.

- By comparing the results for Cases 1–3, it was shown that the higher enrichment plays the dominant role in the UCO fueled core's reactivity behavior, and not the change to UCO fuel kernels.
- The reactivity insertion values for 600 kg of steam was also compared with the reactivity added from a full control rod withdrawal, as was done for the HTR module SAR. A full withdrawal lead to an increased steam ingress value of 1.21% vs. 0.99% for Case 1, compared with values of 1.49% vs. 1.42% for Case 3. The control rod withdrawal event for both these cases (UO_2 and UCO fueled cores) is therefore the limiting/bounding case for reactivity insertion, supporting the original HTR module design intentions.

The analysis of these two accidents, together with the acceptable results obtained from the steady-state and the control rod worth analysis, provided sufficient insight into the behavior of the UCO-fueled HTR module design to conclude that it is a feasible design option that stays within all the reactor physics critical safety envelopes. That said, the actual fuel performance of this core design was beyond the scope of this study, and care should be taken not to equate acceptable neutronics and thermal fluid behavior with acceptable levels of fission product release rates, since many more factors are involved in this aspect of fuel design.

5. REFERENCES

1. G. Lohnert, "Technical Design Features and Essential Safety-Related Properties of the HTR-Module" *Nuclear Engineering and Design*, Vol. 121, pp. 259-275, 1990.
2. D. Matzner, "PBMR Project Status and the Way Ahead", *Proceedings of the 2nd International Topical Meeting on High Temperature Reactor Technology*, Beijing, China, September 22-24, 2004.
3. Z. Zhang, et al., "Current status and technical description of Chinese 2×250 MW_{th} HTR-PM demonstration plant", *Nuclear Engineering and Design*, Vol. 239, pp. 1212-1219, 2009.
4. H. Reutler, "Plant Design and Safety Concept of the HTR-Module," *Nuclear Engineering and Design*, Vol. 109, pp. 335-340, 1988.
5. C. Barnes, "AGR-2 Fuel Specification", SPC-923, Rev. 3, Idaho National Laboratory, 2009.
6. J. Wang, "An Integrated Performance Model for High Temperature Gas Cooled Reactor Coated Particle Fuel", PhD Thesis, Massachusetts Institute of Technology, 2004.
7. W. Terry, H. Gougar, and A. Ougouag, "Direct Deterministic Method for Neutronics Analysis and Computation of Asymptotic Burnup Distribution in a Re-circulating Pebble-Bed Reactor," *Annals of Nuclear Energy* 29 (2002) 1345 –1364.
8. E. Teuchert, U. Hansen, and K. Haas, "VSOP – Computer Code System for Reactor Physics and Fuel Cycle Simulation," Kernforschungsanlage Jülich, JÜL-1649, March 1980.
9. W. Yoon, "COMBINE-6 Cycle 1," WYY-01-94, Idaho National Engineering Laboratory Internal Memo, 1994.
10. H. Gougar, W. Yoon, A. Ougouag, "Multi-scale Analysis of Pebble Bed Reactors", *Proceedings of HTR 2010*, Prague, Czech Republic, 2010.
11. H. Gougar, et al., "Automated Design and Optimization of Pebble Bed Reactor Cores", *Nuclear Science and Engineering*, Vol. 165, Nr. 3, pp. 245-269, 2010.
12. G. Strydom, "TINTE Uncertainty Analysis of the Maximum Fuel Temperature During a DLOFC Event for the 400 MW Pebble Bed Modular Reactor", *Proceedings of ICAPP 2004*, Paper 4165, 2004.
13. G. Strydom, "Use of SUSA in Uncertainty and Sensitivity Analysis for INL VHTR Coupled Codes", INL/EXT-10-19023, 2010.
14. G. Lohnert, "The Consequences of Water Ingress into the Primary Circuit of an HTR-Module – From Design Basis Accident to Hypothetical Postulates" *Nuclear Engineering and Design*, Vol. 134, pp. 159-176, 1992.